Near-infrared Contrast Agents for Cell Type Identification and Detection Utilizing Photoacoustics

by

Joel Lusk

A Dissertation Presented in Partial Fulfillment
of the Requirements for the Degree
Doctor of Philosophy

Approved April 2022 by the
Graduate Supervisory Committee:

Barbara S. Smith, Chair
Rolf Halden
Trent Anderson

ARIZONA STATE UNIVERSITY

May 2022

ABSTRACT

The imaging and detection of specific cell types deep in biological tissue is critical for the diagnosis of cancer and the study of biological phenomena. Current high-resolution optical imaging techniques are depth limited due to the high degree of optical scattering that occurs in tissues. To address these limitations, photoacoustic (PA) techniques have emerged as noninvasive methods for the imaging and detection of specific biological structures at extended depths *in vivo*. In addition, near-infrared (NIR) contrast agents have further increased the depth at which PA imaging can be achieved in biological tissues. The goal of this research is to combine novel PA imaging and NIR labeling strategies for the diagnosis of disease and for the detection of neuronal subtypes. Central Hypothesis: Utilizing custom-designed PA systems and NIR labeling techniques will enable the detection of specific cell types *in vitro* and in mammalian brain slices. Work presented in this dissertation addresses the following: (Chapter 2): The custom photoacoustic flow cytometry system combined with NIR absorbing copper sulfide nanoparticles for the detection of ovarian circulating tumor cells (CTCs) at physiologically relevant concentrations. Results obtained from this Chapter provide a unique tool for the future detection of ovarian CTCs in patient samples at the point of care. (Chapter 3): The custom photoacoustic microscopy (PAM) system can detect genetically encoded near-infrared fluorescent proteins (iRFPs) in cells *in vitro*. Results obtained from this Chapter can significantly increase the depth at which neurons and cellular processes can be targeted and imaged *in vitro*. (Chapter

4): Utilizing the Cre/lox recombination system with AAV vectors will enable selective tagging of dopaminergic neurons with iRFP for detection in brain slices using PAM. Thus, providing a new means of increasing the depth at which neuronal subtypes can be imaged and detected in the mammalian brain. Significance: Knowledge gained from this research could have significant impacts on the PA detection of ovarian cancer and extend the depth at which neuronal subtypes are imaged in the mammalian brain.

ACKNOWLEDGMENTS

I want first to thank my advisor Dr. Barbara Smith. She has stood by me through many of my failures and has constantly pushed me to be a better scientist. I would have never been able to complete this dissertation without her help. I also want to thank my committee members, Dr. Trent Anderson and Dr. Rolf Halden. They both gave me fantastic advice regarding the research in this dissertation. I am forever grateful for their guidance.

I also want to thank all the students in the Smith lab. Dr. Christopher Miranda is an extraordinarily talented and intelligent scientist whose technical knowledge was vital to the completion of this dissertation. I have also had the privilege of seeing Jarrett Eshima transition from his undergraduate degree to being a Ph.D. student in our lab. He is truly one of the most talented and rigorous scientists I know. Ethan Marshall's contributions were paramount to this work, and he is honestly one of the most gifted engineers I have worked with. I had the privilege of working closely with Madeleine Howell, whose innate intelligence and curiosity were astounding. She helped with much of the nanoparticle synthesis in Chapter 2. Tina Aridi is one of the most responsible, consistent, and intelligent students I have seen come through the lab. Tina's help was vital to completing the aims set out in chapter 3 of this dissertation. I not only consider all of you colleagues but lifetime friends.

I would also like to thank all the students, post docs, professors, and research scientists who were always there to provide advice or just commiserate over failed

experiments. Special thanks to the people from DACT including Julianne Daggett-Vondras, Jacki Kilbourne, Kenneth Lowe, and Lindsay Reno for the outstanding care you give to all the animals at ASU.

Also, a huge thanks to my family for supporting me throughout the Ph.D. To my mom for always being there when I needed her. I honestly couldn't ask for a more amazing mother. I would also like to thank my dad for always checking in. You will never know how much those weekend phone calls meant to me. I owe a huge amount of thanks to my sisters for being an inspiration and giving me the best nieces and nephews I could ever ask for. Whenever I would struggle, I would just think about how amazing, funny, and intelligent they all were, and it would inspire me to carry onward.

Finally, I would like to thank my wife, Ariella. She stood by me despite the many years of odd hours, grumpy moods, exasperation, and the highs and lows of research. I often think that she deserves a Ph.D. as much as I do. I cannot imagine anyone who could have been more supportive towards me throughout this process, and without her, none of this would have been possible. I love you more than you could ever comprehend.

TABLE OF CONTENTS

CHAPTER Page

CHAPTER Page

CHAPTER Page

LIST OF FIGURES

Figure Page

Figure Page

Figure Page

Figure Page

Figure Page

Figure Page

Chapter 1

INTRODUCTION

The overarching goal of this dissertation is to develop photoacoustic (PA) systems utilizing near-infrared (NIR) contrast agents to expand cell type detection and imaging for in vitro applications and in mammalian brain slices. The resulting data from this dissertation could significantly advance the fields of ovarian cancer detection and cell type detection of neurons in the brain. This is demonstrated by the development of key technologies for PA detection in concert with NIR contrast agents demonstrated in the subsequent chapters. The custom photoacoustic flow cytometry (PAFC) system outlined in this proposal has the potential to advance the point-of-care diagnosis and management of ovarian cancer. The use of photoacoustic microscopy (PAM) in combination with NIR proteins for cell type detection enables the ability to analyze neuronal subtypes at increased depth, thus enabling more effective methods of imaging neuronal dynamics deep in the mammalian brain.

1.1 Overview

Labeling and imaging specific cell types deep in biological tissue is critically important for the early diagnosis of disease and to study fundamental biological processes. Current imaging strategies lack the depth of penetration necessary to target specific cell types *in vivo* and within patient samples due to endogenous absorbers

that attenuate the penetration depth of light. The diffusion of light in tissues limits the ability to image specific cell types deep within tissue for the diagnosis of disease and study of distinct cellular processes. PA systems, which utilize both light and acoustic feedback, overcome these technical challenges by expanding the depth at which cell types can be detected and imaged in tissues.[141] Recently, new classes of near-infrared (NIR) contrast agents, including near-infrared fluorescent proteins (iRFPs) and inorganic copper sulfide nanoparticles (CuS NPs), have been utilized for PA imaging.[29,60] These NIR contrast agents can be targeted to specific cells utilizing ligands and genetic expression strategies.[107] When used in combination with these NIR absorbers, PA has the potential to surpass current capabilities to noninvasively image and detect distinct types of cells at increased depth in biological samples. Here we propose various targeting and detection strategies combined with NIR absorbing contrast agents for cell type detection *in vitro*. Advantages of these targeted contrast agents include the ability to: 1) Detect ovarian circulating tumor cells in flow at physiologically relevant concentrations using PAFC, 2) facilitate dual PA detection and fluorescence imaging of iRFP in neuronal cells *in vitro* and, 3) enable the PA detection of genetically encoded NIR contrast agents within specific neuronal subtypes in the mammalian brain. These technologies leverage NIR contrast agents and innovative PA techniques for cell type-specific detection.

1.2 Photoacoustic effect

The PA effect is generated when light is absorbed by molecules creating a thermally induced pressure expansion that leads to the propagation of acoustic waves (Fig. 1.1).[132] These acoustic waves can then be detected by ultrasound transducers and the signals can be used to reconstruct images or detect absorbing molecules. Because acoustic waves travel more easily through tissue than photons, imaging techniques utilizing the PA effect can detect structures at increased depth in complex biological mixtures over other optics-based methods.[142] Over the last decade, work on PA imaging and detection strategies in biomedical applications has made great progress in the area of PA tomography (PAT) ranging from the scale of organelles to organs.[133,35,152] This progress has led to imaging and detection modalities that have a greater depth of penetration into biological tissue.

1.3 Photoacoustic Tomography

PAT utilizes the PA effect to produce 2D and 3D images of biological structures at various scales.[68] Utilizing the PA effect for imaging allows PAT to overcome the ballistic regime of photons in tissues allowing for deeper imaging.[132] In addition to overcoming the scattering of photons in tissues, PAT also has the advantage of exploiting the specific absorption of chemical compounds at different wavelengths, allowing for the stimulation of various biological structures.[154] This ability to exploit the chemical absorption of compounds at various wavelengths allows for imaging

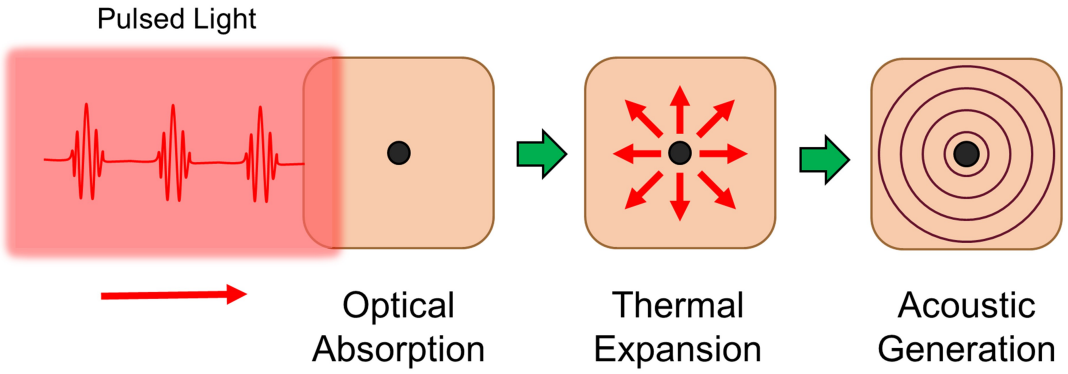

Figure 1.1: Diagram Demonstrating the Generation of the Photoacoustic Effect.

blood, lipids, cytochromes, and other endogenous compounds.[151,15,158,117] In addition, PAT can be utilized with PA contrasts agents to label tissues and cells of interest.[135] These contrast agents allow for the application of PAT across various fields, including neuroscience and cancer detection.[10,89] Currently, PAT systems can be divided into three main categories: photoacoustic computed tomography (PACT), photoacoustic endoscopy (PAE), and photoacoustic microscopy (PAM).[132] The scalability of PAT and its ability to target various molecular structures make it an ideal tool for the investigation of biological structures and its application in the detection of disease states.

1.3.1 Photoacoustic Computed Tomography

On the macroscopic and microscopic scales, PACT has been utilized extensively to examine vasculature, endogenous chromophores, and cells tagged with exogenous contrast agents.[77,153,69] Because of the specific absorption of oxygenated and deoxygenated hemoglobin at different wavelengths, this technology has been applied extensively to detect vasculature endogenously.[72,138] In PACT, the target area is stimulated by unfocused laser light, and the resulting acoustics is detected using an array of transducers.[65] This method sacrifices optical resolution; however, it provides an improved method of deep tissue imaging beyond that of other optics-only based methods. This approach has allowed for the investigation of blood vasculature associated with cancer and studies of the brain.[77,94] This endogenous absorption also enables complete small animal imaging by PA.[71] Using advanced systems with arrays of transducers whole mice can be comprehensively imaged *in vivo*.[71] In addition, this technology has been used extensively to examine vasculature in clinical settings, such as whole breast imaging for the identification of breast cancer.[76]

1.3.2 Photoacoustic Endoscopy

Medical imaging techniques have employed endoscopy to gain access to organs and structures deeper in the body than that of traditional methods. Medical endoscopy has become an important test for diagnosing many diseases, including esophageal and pancreatic cancers.[61,43] PAE employs the properties of PAT to image vasculature and

other endogenous absorbers and through endoscopy extends its reach to previously inaccessible locations.[154,146] In addition, combining endoscopy with PAT allows for the visualization of tissues and organs at higher spatiotemporal resolution. PAE has been utilized in various applications, including the imaging of vasculature in uterine tissues and the esophagus.[145,90] In addition, PAE systems can allow access to structures deeper in the body, such as the aorta and allow for the remote viewing of biological processes in other parts of the body.[40]

1.3.3 Photoacoustic Microscopy

PAM is an *in vitro* and *in vivo* imaging technique that has been utilized to detect blood oxygenation, cellular structures, and exogenous contrast agents at microscopic scales.[150,137,93] PAM takes advantage of the weak scattering of ultrasound waves within tissue which allows it to surpass the optical diffusion limit of traditional microscopy systems.[152] There are currently two characterizations of PAM based on their acoustic and optical foci, including, optical-resolution PAM (OR-PAM) and acoustic resolution PAM (AR-PAM).[50] The penetration depth and the resolution of these systems depend on the optical ballistic regime that governs their use.[50] OR-PAM relies on the alignment of acoustic and optical systems as seen in Fig. 1.2, and the sensitivity is maximized when the foci of these systems are confocally aligned. Therefore, the resolution of OR-PAM is determined by the diffusion of light in tissues or the optical diffusion regime, and can typically view structures up to a depth of 1-2 mm.[152] In the case of AR-PAM, the resolution of the images is based on acoustic focus size.[80]

Typically, these systems use weakly focused light, which allows for structural imaging at depths of 3 mm with a lateral resolution of 45 µm.[160] The resolution of these systems, however, is limited as the depth is increased.[152] In this dissertation, we utilize PAM in combination with iRFP for the detection of neuronal cells *in vitro* and in brain slices.

OR-PAM has been used to image histological sections independent of exogenous contrast.[158,137] Because of the spectral profiles of different cytochromes, lipids, melanin, and blood, OR-PAM can be performed on histological sections that have not been stained.[137] Targeting these unique spectral profiles has led to OR-PAM studies demonstrating performance and resolution similar to traditional H and E staining techniques using endogenous contrast.[137] These studies could lead to possible alternatives to long and complex H and E staining procedures. In addition, OR-PAM has been utilized to image vasculature and determine the oxygen saturation of tumors in animals.[47] Because of its ability to acquire PA images at optical resolution, OR-PAM can image structures down to the level of organelles (ie: cell nuclei).[47,148] This technique has been applied to image individual blood cells and angiogenesis.[78,157] The unprecedented detail provided by the high resolution of OR-PAM combined with its ability to image a variety of endogenous absorbers and exogenous contrast agents makes it an ideal imaging modality imaging biological structures.

For AR-PAM, the imaging depth is greatly based on the acoustic foci of the focused ultrasound transducer being utilized.[152] In addition, by utilizing a weakly

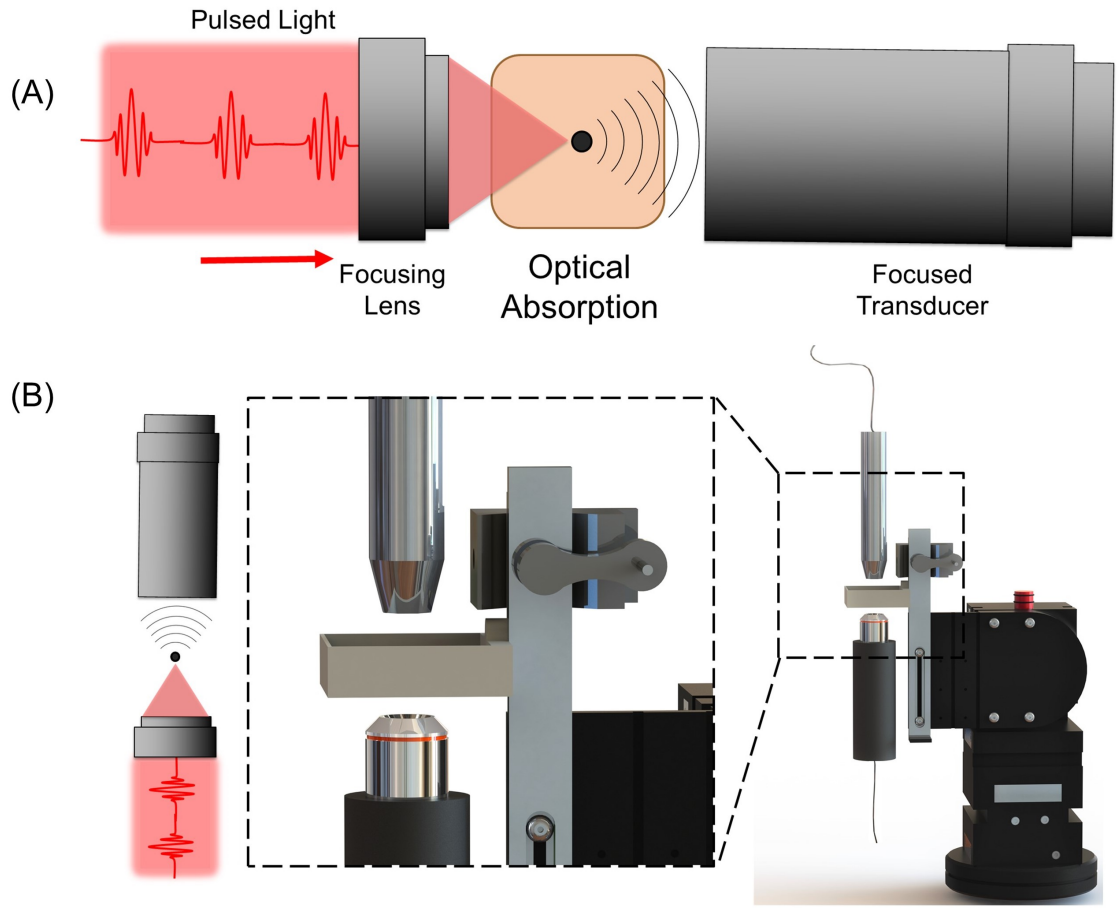

Figure 1.2: (A) Demonstration of Confocally Aligned Optical and Acoustic Foci.(B) Diagram of a Simple OR-PAM Microscopy System.

focused beam of light, chromophores deep within tissues can be stimulated, and their PA response measured using one or more ultrasound transducers.[152] Due to this unique property, AR-PAM systems can image several mm in tissues, though their resolution worsens as the depth increases.[152] This has led to the ability to image tumors deep within tissue.[143] In addition, one study showed the AR-PAM systems' ability to non-invasively image cortical vasculature *in vivo*.[121] With the wide range of PAM systems and their scalability of imaging and resolution, PAM has emerged

as a powerful tool for investigating cellular dynamics and disease states.

1.3.4 Photoacoustic Flow Cytometry

Recently, PAFC has emerged as an effective method for the non-invasive detection of cancer cells, analysis of nanomaterials, and identification of bacteria.[36,95,164] PAFC differs from traditional flow cytometry by detecting analytes in flow using PA instead of fluorescence. PAFC, therefore, has the ability to penetrate more deeply into tissues and biological mediums than fluorescence techniques. Advantages of PAFC over traditional flow cytometry methods include simplicity, ease of translation to clinical settings, and the feasible detection of CTCs at depths of several centimeters in patient samples.[35,99] Recent studies have utilized PAFC systems for the detection of cells using endogenous and exogenous contrast.[13,33] NIR light-absorbing contrast agents such as indocyanine green (ICG) dye and metal NPs (e.g. gold and CuS) have been used for the selective labeling of cells and tissues in combination with PA imaging.[60,42,57] Due to the improved penetration depth of NIR light within biological tissues, PA detection of absorbers can be performed at greater depths for clinical applications. The combination of targeted NIR contrast agents with PAFC has generated considerable interest in detecting CTCs and other targets.

PAFC systems take advantage of different aspects of the PA effect as is seen in a wide range of biological applications. *in vitro* PAFC and flowmetry systems have been utilized for many different applications, including the detection of melanoma cells and cancer cells utilizing metal nanoparticles.[32,129] The advantage of this tech-

nique over traditional fluorescent flow cytometry is its ability to detect cells in more complex biological mixtures and its ability to use endogenous contrast. Because of the improved penetration depth of PA, these systems can potentially be used to evaluate complex biological mixtures for the presence of circulating tumor cells without the use of expensive fluorophores. Furthermore, the simplicity of PAFC makes it an ideal candidate for use in resource-poor settings. Finally, many of these PAFC systems have a great potential to detect nanoparticle and endogenous circulating cells in tissues which could further improve clinical diagnostics and nanoparticle research *in vivo*.

Other iterations of PAFC include *in vivo* applications where cells and other analytes can be analyzed within the vasculature of a living animal.[35] This takes advantage of the PA effect which enables deeper penetration into tissues, allowing for the characterization of analytes within the circulatory system.[35] This approach has several advantages over traditional flow cytometry because cells can be analyzed *in vivo*. For example, a study utilized concentrated magnetic nanoparticles *in vivo* to create a higher PA signal.[34] This tool enables the observation of cells and other analytes to be observed in a physiologically relevant environment and further traced to their direct source in the circulatory system. In summary, PAFC has many advantages over traditional flow cytometry for both *in vitro* and *in vivo* settings, where it can be utilized for a variety of important biological applications. In this dissertation, we utilize PAFC in combination with folic acid capped CuS nanoparticles for the detection of

ovarian cancer cells.

1.4 Photoacoustic Contrast Agents

PA contrast agents allow researchers to extend the depth and specificity of PA imaging.[140] These contrast agents are generally tuned to absorb light in the NIR to maximize the depth of imaging and detection that is possible using PA (Fig. 1.3).[135,140] NIR PA contrast agents can be synthesized from a variety of materials including; organic and inorganic nanoparticles, small molecule dyes, and genetically encoded proteins.[81,74,54,59] These contrast agents have been designed for a multitude of applications including cell tracking, tumor detection, and protein-protein interactions.[28,83,67] Utilizing these techniques has allowed researchers to move beyond endogenous targeting to label specific cell types and processes at enhanced depth in biological systems.

1.4.1 Endogenous Contrast

Because of its optical to acoustic conversion properties, PA imaging can utilize a variety of endogenous contrast. The most widely used endogenous PA agents include hemoglobin and deoxyhemoglobin. Because of the absorption shift of hemoglobin in oxygenated states and deoxygenated states, PA can be employed not only for the detection of blood structures, but also for the identification of the change of blood oxygenation and hypoxic states.[141] This strategy has been used extensively in the study of cancer, which has a characteristic increase in tumor vasculature.[142] In addition,

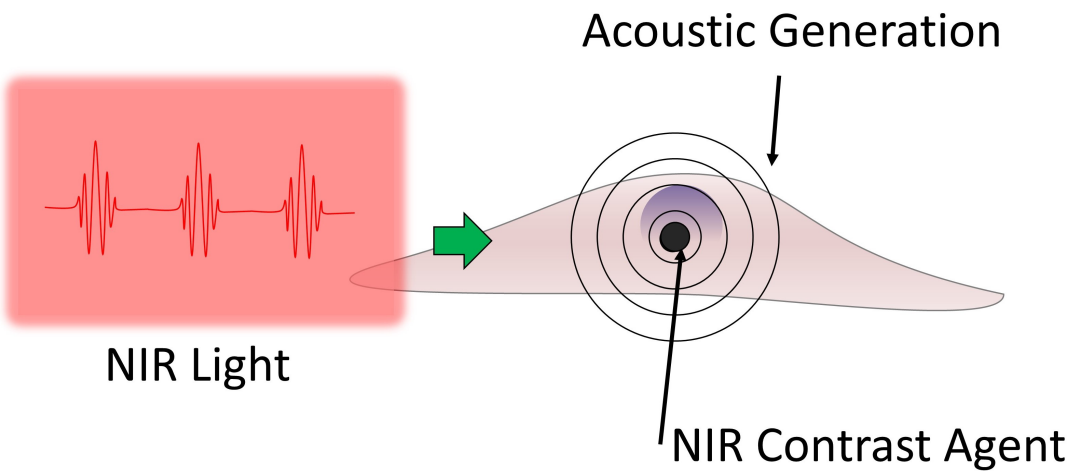

Figure 1.3: Diagram of the Generation of the Photoacoustic Effect from Pulsed Light Stimulating an NIR Contrast Agent Tagged Cell.

this has been explored in neural applications through the movement of oxygenated and deoxygenated blood to different regions of the brain in response to stimuli.[150] In addition to blood, several other endogenous contrast agents have the characteristic ability to produce the PA effect, including melanin, lipids, and nucleic acids.[65,148,108] These properties have been exploited to detect melanoma cells and label-free microscopy of nuclei through the absorption of DNA and other structures.[148,130] The endogenous characterization of structures using PA is one of the greatest strengths of PA imaging and can be further leveraged when combined with other modalities and contrast agents to investigate biological processes.

1.4.2 Small Molecule Dyes

Small molecule dyes have been used in PA imaging and can be tuned to the NIR to absorb light deep in tissues. These dyes have a typical structure which incorporates small, highly conjugated, aromatic ring systems.[135] One of the primary candidates that have been extensively studied for small molecules is indocyanine green. ICG is a heptamethine cyanine dye that is FDA approved and has low toxicity *in vivo*.[135] Its absorption maximum at 780 nm makes it a good candidate for imaging deep within tissues. Though ICG has shown great promise for tumor cells, its low photostability and difficulty in being conjugated to targeting modalities makes it less useful for targeted PA imaging of structures in the body.[16,135] Other small molecule dyes that have also been explored are squaraines, rhodamines, and azo dyes.[135] However, these dyes are not as commonly studied due to their limitations as compared to heptamethine cyanine dyes. Though these small molecules can be helpful for PAI, primarily because of their low toxicity and the FDA approval of ICG, they have several properties that limit their usefulness, including their very low molar extinction coefficient, low solubility, tendency to aggregate, and low photostability.[135] Despite their disadvantages, these dyes have been extensively studied in relation to the biodistribution of different cell types and the detection of epidermal growth factor receptor expression when combined with PAI.[109,28]

1.4.3 Inorganic

The most researched inorganic contrast agents for PA imaging are metallic nanoparticles. This class of particles is popular because of their high degree of customizability regarding size and wavelength absorption and their high molar extinction coefficients, which allow for the high photothermal conversion of light to an acoustic signal.[140] In addition, these metallic nanoparticles can be conjugated to a variety of ligands to target cells and molecular structures of interest. The most highly explored inorganic nanoparticles are gold. Gold nanoparticles have been extensively explored for PA imaging and many other biomedical applications.[75] Gold nanoparticles, which can be tuned to NIR wavelengths, come in various shapes, including nanorods, nanospheres, nanoshells, and nanostars.[75] These nanoparticles can also be made biocompatible with a variety of coatings (i.e.: silica encapsulation, pegylation).[140,25] Over the last few decades, many studies have utilized these metallic nanoparticles for PA and biomedical imaging applications; however, few of these nanoparticle systems have made it to the clinic.[75,119,25]

Another inorganic compound, CuS has also been used extensively in PA imaging. Copper sulfide nanoparticles have emerged as an easily synthesizable contrast agent for PAI with wavelengths that can be tuned to >1000 nm.[166] In addition, like gold nanoparticles, CuS nanoparticles can be capped with citrate or folic acid, allowing it to be conjugated to a variety of other reagents such as PEG for improved biocompatibility.[165] Furthermore, CuS nanoparticles can also be capped with targeting ligands

such as antibodies to target cells of interest.[37] In this dissertation, we utilized folic acid capped CuS nanoparticles for the detection of ovarian cancer cells in a custom PAFC system.

1.4.4 Organic and Carbon Based

The organic subclass of PA contrast agents includes conjugated polymer nanoparticles, graphene, and carbon nanotubes.[31] Polymer nanoparticles have recently shown extensive promise in PA imaging for their high PA signal generation and biocompatibility. These contrast agents can be tuned to have strong absorption in the NIR.[135] Polymer-based compounds can also be aggregated into nanoparticle-based contrast agents, with high molar extinction coefficients. Overall, these polymeric nanoparticles have shown great promise as future PA contrast agents, though research in this area is still in its early stages.[135]

The two main classes of organic PA contrast agents used for PA imaging are carbon nanotubes and graphene-based nanomaterials. These materials are particularly suited for PA imaging due to their absorption properties in the NIR window.[23,155] Single-walled nanotubes (SWNTs) exhibit a broad absorption peak but can be additionally tuned to have strong absorption in specific wavelengths when conjugated with other molecules.[31,23] Though SWCNTs are cytotoxic on their own, they can be coated with noble metals to increase their biocompatibility and PA signal generation in specific wavelengths.[55] Graphene-based nanomaterials that are also carbon-based, are typically added in combination with other metal-based contrast agents to increase the

PA signal.[31,92] The increased PA effect is due to the graphene layer which enhances the thermoconductivity of these nanoparticles.[31] These carbon-based nanoparticle systems show exceptional potential when combined with other nanoparticle and small molecule contrast agents.

1.4.5 Genetically encoded

Through the work of pioneering scientists such as Osamu Shimomura, Martin Chalfie, Douglas Prasher, and Roger Tsien, fluorescent proteins have been utilized to visualize protein expression in cells.[106,17,116] Since the first expression of green fluorescent protein (GFP) in cells, these genetic probes have revolutionized the ability to visualize gene expression.[125] However, the use of reporter proteins is not unique to fluorescence and proteins have been utilized to generate contrast across a wide range of imaging modalities, including ultrasound, MRI, and PA.[112,144,12] Fluorescent proteins have been further engineered to fluoresce in a broad range of colors by Roger Tsien and others.[113,14,45] The green fluorescent protein itself can be utilized for PA studies; however, it is not sufficiently red-shifted to be useful in biological tissue.[24] Examples of RFPs have also been shown in PA research, however, fluorophores with absorbance shifted into the NIR have been identified as the most advantageous.[24]

Recent studies have utilized a new class of genetic fluorophores, called near-infrared fluorescent proteins (iRFPs).[30] These iRFPs are engineered from bacterial phytochromes.[30] One of the first proteins to be utilized was iRFP713, with a peak light excitation at 690 and emission at 713.[30] This protein has been used extensively

in PA studies for the detection of tumor cells *in vivo*.[29,30] In addition to these initial experiments with iRFP, new bacterial phytochromes have been developed, including photoswitchable iRFP proteins and monomeric iRFPs that can be used in conjunction with PA.[149] Photoswitchable iRFPs can be switched from a trans to cis configuration by introducing specific wavelengths of light. This conformational change shifts the absorption characteristics of the iRFP.[149] Utilizing this photoswitching strategy, researchers can limit the background signal and improve the sensitivity of PA imaging.[149] In addition, monomeric iRFPs have been utilized to visualize protein interactions with PA.[67] IRFP has also been used extensively in biological studies and for neuroscience applications where it can be fused to optogenetic structures and modified to target organelles.[107] Overall, iRFP and its many variations have significantly expanded the capabilities of molecular PA imaging. In this dissertation, we aim to use iRFP in combination with a custom designed PAM system to detect specific neurons.

Other genetic approaches involve the expression of PA contrast using endogenous absorbers through enzymatic reactions. One key example of this is the use of the enzyme tyrosine kinase, which leads to melanin production in non-melanin producing cells.[105] Because of the high PA signal generated by melanin, this strategy has been used to image cells *in vivo*.[105] In addition, the LacZ reporter in combination with X-gal has been used for PA imaging. LacZ, when combined with X-gal, produces a dark dye that has been detected at increased depths *in vivo*.[70] This system has recently been used to visualize neuronal expression when linked with the fos reporter

in the mouse brain.[88] Overall, these enzymatic strategies to produce PA contrast have proven effective for extending the reach of PA techniques in biological tissue.

1.5 Targeting Ligands

A variety of targeting moieties have been developed to identify cells and structures of interest utilizing PA. These include small molecules, peptides, aptamers, antibodies, and proteins. Targeting molecules have been applied for targeting stem cells and a variety of diseases. These ligands can be customized for a specific target and the contrast agent they are conjugated to. Targeting moieties greatly expand the capabilities for PA imaging and detection by directing the contrast agents to targets of interest. Here we review several of these techniques for PA detection.

1.5.1 Small Molecules

One of the most widely used strategies for targeting nanoparticles and other contrast agents utilizes small molecules for targeting cell surface receptors. The significant advantages of these small molecules include their stability, ease of conjugation, and low cost to synthesize.[20] One of the most widely used small molecules for cancer targeting is folic acid.[20,4] Folic acid has a high affinity for the folate receptor, an endogenous cell receptor. This folate receptor is highly expressed in several cancer subtypes, including ovarian cancer.[86,4] When folic acid attaches to this cell surface receptor, it is taken into the cell via receptor-mediated endocytosis.[4] This uptake makes folic acid an ideal candidate for contrast agents to detect ovarian cancer cells. Folic

acid conjugated contrast agents have been utilized for a variety of imaging modalities for ovarian cancer.[159,38] Though there are a few highly advantageous small molecule compounds such as folic acid, the majority of small molecules lack the specificity to be used extensively in PA imaging. In our studies, we utilize folic acid conjugated CuS NPs for the detection of ovarian cancer cells in a custom PAFC system.

1.5.2 Antibodies

Antibodies with their high specificity for antigen targets are ideal molecules for conjugation to PA contrast agents for targeting various diseases. Within the immune system of animals, antibodies have evolved to have high specificity for antigens to neutralize pathogens. Because of this high specificity, antibodies have been utilized to target contrast agents for a variety of imaging modalities including MRI, ultrasound, PET, and PA imaging.[62,98,11,136] Within PA imaging, antibody conjugated contrast agents have been used to detect cancers and cell surface receptors.[136,73] An additional advantage of antibody targeting systems is their ability to be easily conjugated to various contrast agents. Though they have been extensively studied, antibody conjugation methods still face significant hurdles, including stability, immunogenicity, purity, and circulation time.[20] Despite these challenges, antibodies are one of the most widely used modalities for contrast agent targeting.

1.5.3 Peptides

Peptides, which are strings of aminos acids, are ideal candidates for PA targeting of contrast agents due to their customizability and ease of synthesis.[139] With the advent of peptide phage display and the development of peptide microarrays, the ability to specifically target these ligands to antigens of interest have made peptide-conjugated contrast agents an easy, effective, and accessible approach to researchers.[139,123] Furthermore, small peptides have been utilized to target various cell surface proteins. Within PA, these peptides have been utilized to detect various tumors.[20,52,156,18] Though these peptides show exceptional ability to target cells *in vitro*, their adaptation to *in vivo* studies is more challenging due to problems of proteolysis and immunogenicity.[20] Peptide-based methods show great promise for the targeting of PA contrast agents despite these challenges.

1.5.4 Apatamers

Aptamers are short single-stranded oligonucleotides that can bind to a variety of structures and have become increasingly used in PA imaging.[161,1] Aptamers can be utilized to detect small compounds, proteins, and live cells.[1] DNA and RNA aptamers can be built to identify virtually any target utilizing a technique called SELEX (Systemic Evolution of Ligands by EXponential Enrichment).[126,20,161] They also exhibit low immunogenicity and are modifiable to increase their ability to circulate *in vivo*.[1] These aptamers, however, are degraded by the nucleases present *in vivo*.[1] However,

current research has explored aptamer modification for higher *in vivo* stability.[1]

1.5.5 Genetic Targeting

Genetic targeting of PA contrast has depended mainly on enzymatic expression in cells, which produce cellular byproducts that are PA such as melanin or X-gal.[70,105] The majority of research in genetic targeting has focused on these enzymatic strategies. Research into genetic targeting of cells via other methods is severely lacking. Many genetic tools, especially in neuroscience, have emerged to target cell types for fluorescence imaging. However, few of these methods have been applied to PA techniques. Examples of this include (1) the Cre-Lox system for expression of various molecules within specific cell types within transgenic mice and (2) the rabies-based neuronal tracking to trace neurons throughout the brain.[111,128] Although a genetic toolbox for specific cell targeting exists in other fields, especially in neuroscience, it has not been widely explored in the field of PA.

One of these genetic strategies, known as the Cre-lox recombination system, originally derived from the P1 bacteriophage, which allows for specific control of gene expression within target cell populations.[110,111] Utilizing this system, neuroscientists have been able to study a variety of cellular processes and phenomena in the brain, leading to a greater understanding of the function and relationship of neuronal subtypes.[125] To the best of our knowledge, this system has not been utilized in combination with PAM for the investigation of neurons utilizing iRFP. In this dissertation, we aim to specifically target neuronal subtypes using Cre-lox recombination and detect

them using a custom PAM system, expanding the ways in which neuronal cells can be detected in the mammalian brain.

1.6 Outline of the Dissertation

In Chapter 2, the details regarding the system architecture of the photoacoustic flow cytometry system, synthesis of copper sulfide nanoparticles, and utilizing these nanoparticles to detect cells in flow is described.

In Chapter 3, the motive for utilizing photoacoustic microscopy for the detection of IRFP is discussed. The methods for developing a monoclonal iRFP expressing line is presented. Photoacoustic microscopy data from iRFP cells are presented.

In Chapter 4, the rationale for the use of PAM for the detection of iRFP in mammalian brain tissue is presented. Data showcasing the expression of iRFP in these brain regions is also shown and detection of iRFP in these tissues utilizing PAM is presented.

In Chapter 5, the work from chapters 2-4 is discussed and future directions for this research are proposed.

Text and figures in this PhD dissertation are adapted from previously and soon to be submitted published articles:

- Chapter 2: Reprinted with permission from: **Lusk, J. F.**, Miranda, C., Howell, M., Chrest, M., Eshima, J., Smith, B. S. (2019). Photoacoustic flow system for the detection of ovarian circulating tumor cells utilizing copper sulfide nanopar-

ticles. ACS Biomaterials Science Engineering, 5(3), 1553-1560 Copyright 2019 American Chemical Society.[84]

- Chapter 2: Adapted from: **Lusk, J.F**, Miranda, C. Smith, B.S. "Ovarian Cancer Detection Using Photoacoustic Flow Cytometry." *J.*Vis.Exp. (155) e60279 doiL10.3791/60279 (2020) 19 (2020).[85]

- Chapter 3 and 4: **Lusk, Joel**, et al. "Detection of Neuronal Subtypes Utilizing Genetically Encoded Fluorophores and Photoacoustic Microscopy." *To be submitted*

Chapter 2

PHOTOACOUSTIC DETECTION OF OVARIAN CANCER CELLS UTILIZING COPPER SULFIDE NANOPARTICLES IN FLOW

2.1 Introduction

Ovarian cancer is one of the deadliest gynecological malignancies and resulted in an estimated 184,800 deaths worldwide in 2018.[27] Although advances in first-line ovarian cancer treatments have increased the rates of initial therapeutic success, a vast majority of patients (85−90%) will experience disease recurrence with a median survival time of only 12-24 months.[46,3,87] Disease recurrence often manifests itself through ascite formation, elevated CA125 biomarker levels, and tumor development.[49,58]

Unfortunately, these indicators are detected with variable success or after substantial disease progression, when treatment success is much lower.[48,53] There has been growing interest in the presence of circulating tumor cells (CTCs) as an indicator of patient prognosis.[102] Ovarian CTCs are metastatic cells that detach from the primary tumor and disseminate into intraperitoneal fluid. Although ovarian tumor metastases preferentially grow in the intraperitoneal cavity, these tumor cells also circulate in the peripheral blood supply.[103] In the majority of ovarian epithelial cancers, CTC presence has been shown to precede primary tumor growth, making CTC identification an attractive alternative to current methods of cancer detection.[2] Fur-

thermore, the presence of CTCs in patients with recurrent ovarian cancer has been associated with poorer patient outcomes.[102,26] Thus, CTC detection has the potential to offer diagnostic information as well as inform future treatment for those with ovarian cancer.

Current clinical measures for CTC detection in blood lack the sensitivity for translation to clinical settings for ovarian cancer. Many of these methods, including the CellSearch system, rely on the presence of the EpCAM surface antigen in CTCs.[100] EpCAM, however, is down-regulated in the process of epithelial-mesenchymal transition (EMT), which tumor cells undergo prior to detachment from the primary tumor.[100,39] Furthermore, unlike other epithelial cancers, ovarian cancer's primary mode of metastasis is not hematogenous, and ovarian CTCs enter the peripheral blood circulation in fewer number than those of breast, prostate, or lung cancer.[103] Due to their rarity and the low sensitivity of EpCam, ovarian CTCs can evade detection by traditional enrichment methods.

Folate receptors, which are overexpressed in approximately 90% of ovarian carcinomas, introduce a potentially more sensitive method for CTC detection.[101] Recent studies have reported increased CTC recoveries when using folate receptor targeting instead of EpCAM enrichment methods in ovarian and breast cancer patient blood samples.[44,34] In these reports, nanomaterials and fluorophores functionalized with folic acid are used to generate a photoacoustic (PA) or fluorescence signal for improved CTC detection. A benefit of PA over fluorescence is the ability to detect CTCs more

accurately in whole blood and tissue. In PA imaging, the absorption of nonionizing near-infrared (NIR) radiation by specific organic or inorganic contrast agents induces a localized temperature increase and subsequent thermoexpansion. This thermoexpansion results in the propagation of sound waves from the contrast agent that can be detected with an ultrasound transducer.[90,91] Recently, copper sulfide (CuS) contrast agents have been shown to exhibit excellent NIR absorption and PA signal at depths of 5 cm in biological tissue and enhanced biodegradability and biocompatibility over traditional gold contrast agents.[60,41] These factors, along with the low cost and high photothermal conversion of this material, make folic acid functionalized CuS nanoparticles (NPs) an attractive contrast agent for the detection of ovarian CTCs in clinical and preclinical settings.

In the first chapter of this dissertation, a new method is developed for the detection of ovarian CTCs in a custom PA flow system. This technique utilizes folic acid functionalized CuS NPs (FA-CuS NPs) for the PA detection of CTCs. The photoacoustic flow cytometry (PAFC) system is evaluated through the detection of NPs and tagged ovarian cancer cells within two-phase flow.

2.2 Materials and Methods

2.2.1 Materials

Folic acid and sodium sulfide nonahydrate (Na_2 S$\cdot$ $9H_2O$) were purchased from Sigma-Aldrich (St. Louis, MO, USA). Copper(II) chloride ($CuCl_2$) was purchased

from Acros Organics (Geel, Belgium). Amicon Ultra-4 and Ultra-15 (30 kDa MWCO) centrifugal columns were purchased from EMD Millipore (Burlington, MA, USA). Texas Red-X succinimidyl ester fluorescent dye was purchased from ThermoFisher (Waltham, MA, USA). DAPI (4',6- diamidino-2-phenylindole) was purchased from Molecular Probes (Waltham, MA, USA). Folic-acid-free RPMI 1640 media, McCoy's 5A cell culture media, and the antibiotics penicillin and streptomycin were purchased from Gibco (Grand Island, NY, USA). Fetal bovine serum (FBS) was purchased from Sigma-Aldrich (St. Louis, MO, USA), and trypsin 0.25%, 2.21 mM EDTA 1×, was purchased from Corning (Corning, NY, USA).

2.2.2 Synthesis and Fluorescent Tagging of FA-CuS NPs

FA-CuS NPs were synthesized according to Zhou et al., with minor modifications.[165] Briefly, 100 μL of 1 M Na_2S was added to 100 mL of a 1 mM $CuCl_2$ solution containing 0.16 mg of folic acid at room temperature under constant stirring for 5 min. The reaction was then heated to 90 °C in an oil bath. Once the oil bath reached 85 °C, the reaction was heated for 1 additional hour, gradually turning to a dark green color, and immediately removed from the heat. The FA-CuS NP solution was transferred to an ice bath, allowed to reach temperature, and stored at 4 °C. Prior to concentration and purification of the synthesized NPs, the reaction mixture was raised to a pH of 10. The particles were concentrated using a 30 kDa MWCO centrifugal filter and were washed 4 times with deionized (DI) water (pH ∼10). The particles were then resuspended in PBS and stored at 4 °C until use.

To fluorescently label the FA-CuS NPs, Texas-Red-X succinimidyl ester (0.2 mg dissolved in DMSO) was added to a solution containing 2 mg of FA-CuS NPs in a 0.1 M sodium bicarbonate (pH 9) buffer. The reaction was stirred for 1 h and purified by a centrifugation column by spinning at 4000g for 10 min (30 kda MWCO). It was then washed 3 times with 0.1 M sodium bicarbonate buffer (pH 9) and subsequently with DI water until a negligible concentration of fluorescence was observed in the flow-through.

2.2.3 Characterization of FA-CuS NPs

Absorption of FA-CuS NPs and fluorescence of the Texas Red-X modified NPs were determined using an ultraviolet-visible (UV−vis) and fluorescence spectrophotometer (Molecular Devices, San Jose, CA). The FA-CuS NPs size was measured by transmission electron microscopy (TEM, CM12, Phillips, Tokyo, Japan) at an accelerating voltage of 80 kV. Size distribution of the NPs was determined using dynamic light scattering (DLS, DelsaNano C particle analyzer, Beckman Coulter, Brea, CA). Successful conjugation of the particles to folic acid was determined by time-of-flight/time-of-flight matrix-assisted laser desorption/ionization (MALDITOF/TOF, AB SCIEX 4800, Foster City, CA). The laser power was set to 2825 W/cm2 at 2500 shots/spectrum. Spots were prepared using a 1:1 ratio of sample to α-cyano-4- hydroxycinnamic acid (CHCA) matrix (EMD Millipore). The instrument was run in the positive ion mode at a mass range of 200-1200 Da with a focus mass of 440 Da.

2.2.4 Cell Culture

The cell line SKOV-3 (human ovarian cancer cell) was obtained from ATCC (American Type Culture Collection, Manassas, VA, USA). SKOV-3 cells were cultured in McCoy's 5A medium supplemented with 10% FBS, 100 U/mL penicillin, and 100 μg/mL streptomycin and maintained at 37 °C in a humidified 5% CO_2 incubator. For all experiments cells were incubated in folic-acid free RPMI-1640 media supplemented with 10% FBS, 100 U/mL penicillin, and 100 μg/mL streptomycin. All cells used were at or below passage 7 in this study.

2.2.5 Tagging CTCs for in Vitro Flow Detection

Experiments with tagged cells were performed on SKOV-3 cells that had been incubated in folic-acid-free RPMI-1640 media for at least 24 h. Cells were seeded at a density of 0.05×10^6 cells/mL in a 24 well plate. The following day, cells were incubated with 400 μg/mL of FA-CuS NPs in folic-acid-free RPMI-1640 media for 2 h. Following this incubation, the cells were trypsinized with 0.25% trypsin with EDTA. Folic-acid free RPMI-1640 medium was added, and the cells were centrifuged at 123g for 6 min. Following removal of the supernatant, the cell pellet was resuspended in PBS and centrifuged twice to remove any unbound NPs. Finally, the cells were resuspended in PBS with 2% TWEEN solution and diluted to 1000 cells/mL for subsequent experiments. All cell counts were performed using trypan blue and a hematocytometer

2.2.6 *In-Vitro Cellular Uptake of FA-CuS NPs*

Prior to incubation with fluorescent FA-CuS NPs, cells were seeded on glass coverslips in a 24 well plate at a density of 0.05×10^6 cells per well in folic-acid-free RPMI-1640 media. After 24 h, and at approximately 25% cell confluency, the cells were incubated with fluorescently tagged NP concentrations of 100, 200, and 400 μg/mL in folic-acid-free RPMI media. After incubation at 37 °C for 2 h, all wells were gently rinsed with PBS, fixed with 3.7% formaldehyde, permeabilized with 0.1% Triton-X, and stained with DAPI for cell nuclei identification. The coverslips were then rinsed with PBS and mounted on glass slides using a ProMount Diamond Antifade (ThermoFisher, Waltham, MA). Fluorescence microscopy was performed using a Leica DMI6000B microscope (Leica Microsystems Inc., Buffalo Grove, IL).

2.2.7 *Flow System Architecture*

A schematic of the experimental setup is provided in Figure 2.1. To enable simplicity and usability for clinical settings, the PAFC system is composed of five primary components, including the following: (i) transducer, (ii) laser, (iii) microscope, (iv) flow tank, and (v) pump system. Dual syringe pumps (DUAL-1000 US, New Era Pump) injected both the sample and air simultaneously via 3.1 mm Masterflex platinum cured silicone tubing into a 1.5 mm capillary tube inside of a custom 3D printed flow tank. The sample and air were pumped at rates of 20 and 40 μL/min, respectively. The dual syringe pumps produced two-phase flow with alternating air and

sample zones at volumes of approximately 1 μL increments (i.e., plugs). Within the test setup, the capillary tube was submerged $\sim$9 mm within the flow tank. As the sample passed through the capillary tube, it was irradiated by an optical fiber with a circular beam profile, channeling a diode-pumped solid-state laser (QUANTAS-Q1D-1053, RPMC Lasers Inc.) operating at a wavelength of 1053 nm. The laser provided an excitation light with a fullwidth half-maximum (FWHM) of 8 ns at a pulse repetition rate of 10 Hz. A 10$\times$ objective with a 0.25 numerical aperture (NA) (LMH10X-532, Thorlabs) was used to couple light to a 550 μm diameter multimode optical fiber. The optical fiber was held stationary such that a section of a capillary tube (QF150-75-10, Sutter) was illuminated by the laser with a pulse-energy of approximately 8 mJ. PA signals were detected using an unfocused 50 MHz transducer with an element diameter of 6 mm and a -6 dB fractional bandwidth of 82% (V214-BB-RM, Olympus). The ultrasound transducer was positioned on a glass window inserted into the side of the flow cell, perpendicular to the flow. Acoustic coupling between the glass window and a 50 MHz transducer was achieved using ultrasound gel. Signals detected by the transducer were sent to an ultrasound pulser/ receiver (5077PR Square Wave pulser/receiver, Olympus Inc.). Amplification was performed through a 59 dB gain. A multipurpose reconfigurable oscilloscope (NI PXIe-5170R, National Instruments Corporation), equipped with a built-in field programmable gate array (FPGA), was used for data acquisition. Data was processed and transferred to a computer, where the reconstructed image was displayed in real time as seen in Fig.

2.5. Multipurpose programmable function input/ output lines, built into the FPGA, were used for custom triggering and synchronization of the imaging system. The flow tank was mounted on the stage of an inverted fluorescence microscope (VWR, Bridgeport, NJ), and a viewing port in the base of the cell allowed for the monitoring of cells and contrast agent in flow. The microscope image was recorded using a digital camera (Thorlabs, Austin TX) and used to track the position of the samples as they passed through the flow.

2.2.8 PA Detection of Labeled CTCs

Samples containing dilutions of tagged and untagged SKOV-3 cells were pumped through the system along with 2% TWEEN in PBS as a negative control, and FA-CuS NPs as a positive control. The samples traveling through the capillary tube and across the path of the laser were monitored by a camera and were correlated to the resulting PA signal recorded by the ultrasound transducer. Measurements were taken for samples containing 1000 cells/mL in 2% TWEEN in PBS that had been incubated with FACuS NPs, and the same concentrations of untreated cells in 2% TWEEN in PBS.

2.2.9 Statistical Analysis

Differences in PA signal generation between PBS, 1000 cells/mL, and NP-tagged 1000 cells/mL were compared using Welch's t test after a log transformation of the data. Differences between conditions were considered statistically significant at $p <$

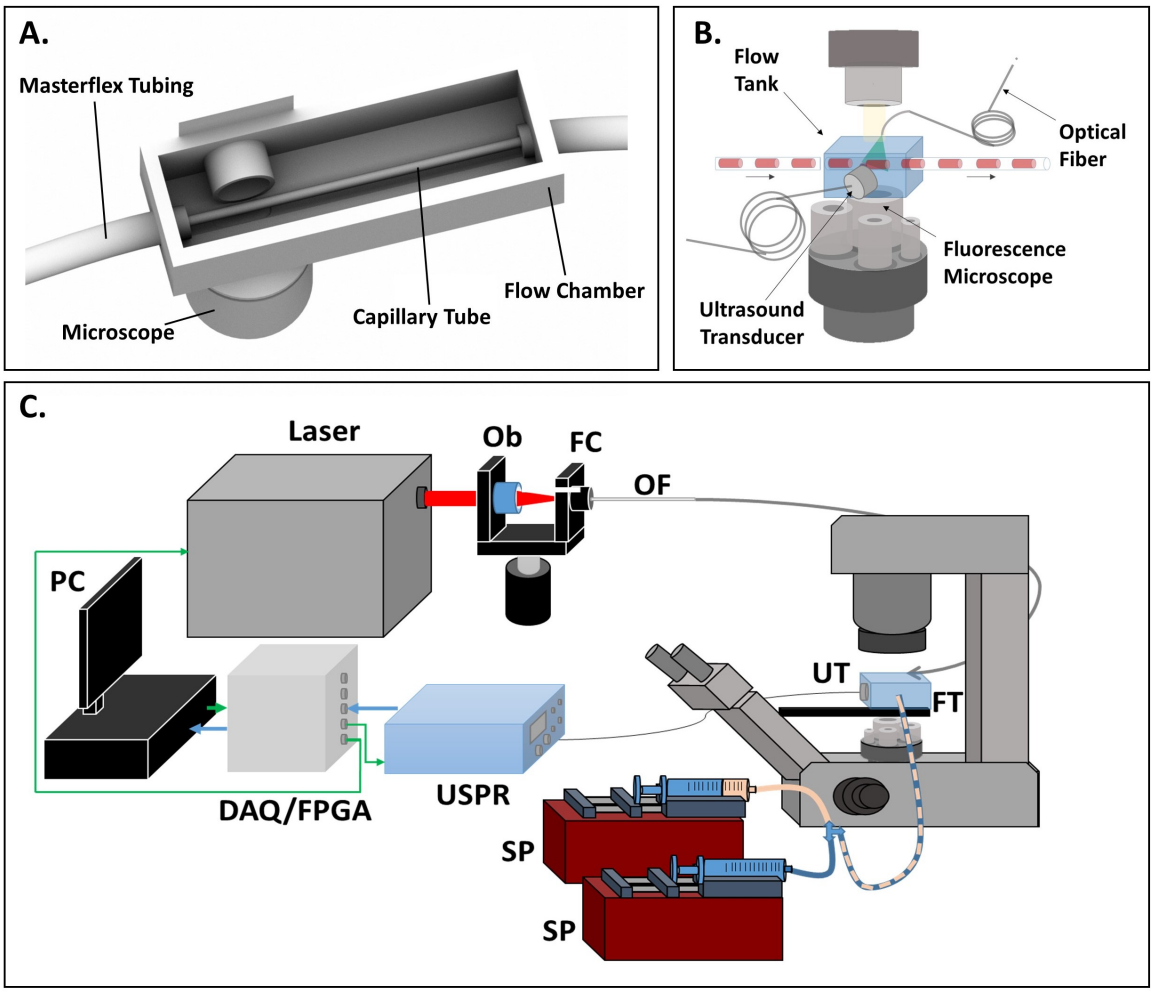

Figure 2.1: Representative Images of Photoacoustic Flow Cytometry System and Flow Chamber. (A) Detailed View of the 3D Printed Flow Chamber. (B) Diagram of PAFC System. (C) Flow System Architecture: SP = Syringe Pump; DAQ/FPGA = Data Acquisition/Field Programmable Gate Array; Ob = Objective Lens; OF = Optical Fiber; FC = Fiber Coupler; UT = Ultrasound Transducer; FT = Flow Tank.

0.05. Statistical tests were run using R statistical software

2.3 Results And Discussion

The sensitive detection of ovarian CTCs could potentially increase the early diagnosis of ovarian cancer metastasis and prolong the lives of those suffering with this devastating disease.[166] Current strategies to identify and isolate CTCs from patient samples include microfluidic devices,[64,51,97] real time PCR (RT-PCR),[8,21,22] and flow cytometry.[6,82] Among these, flow cytometry has been shown to be one of the most promising technologies for the detection and isolation of CTCs, having the ability to classify CTCs by multiple parameters simultaneously.[134,124] However, the use of traditional flow cytometry for *in vivo* applications is limited by the poor penetration of light through tissues.[35] PAFC combines traditional flow cytometry with PA detection to characterize CTCs in flow.[35] Several studies have demonstrated the value of PAFC for its ability to isolate and identify specific cells using either endogenous or exogenous chromophores to generate contrast.[7,13] PAFC has several advantages over traditional flow cytometry including its ability to specifically identify cells of interest deep in human tissues and its ease of translation to in vivo applications.[35] These PAFC systems show great promise; however, to the best of the authors' knowledge, no study has yet utilized PAFC for the detection of ovarian CTCs. In this work, we use NIR absorbing FA-CuS NP contrast agents in combination with a custom PA flow system to detect ovarian CTCs.

2.3.1 Synthesis and Characterization of FA-CuS NPs

CuS NPs with their ease of synthesis, low cytotoxicity, biodegradability, and absorption in the NIR are ideal for PA applications. Therefore, we have synthesized FA-CuS NPs and utilized these contrast agents for the specific detection of ovarian CTCs within our custom flow system. We produced FA-CuS NPs with characteristic NIR absorption from CuS as shown in Fig.2.2D. This absorbance in the NIR allows the NPs to be irradiated deep in tissues, making them an ideal candidate for *in vivo* applications. In order to further characterize the NPs we utilized TEM, DLS, and MALDI-TOF-MS. Figure 2.2A shows a TEM image of the FA-CuS NPs which is representative of the size and distribution of the NPs. TEM measurements were performed manually utilizing ImageJ. To more accurately measure size, the images were thresholded, and a watershed function was applied to separate the particles for measurement. The size of individual NPs (n = 200) was quantified by taking measurements of the vertical and horizontal diameters perpendicular to one another. The two diameters were averaged for each of the NPs to more accurately represent the individual FA-CuS NP diameter. The measured size distribution can be seen in Fig. 2.2B, where the average measured mean diameter from TEM was approximately 8.6 nm. The particles were analyzed by DLS showing an averaged cumulative hydrodynamic diameter of 73.6 nm and a representative measurement is shown in Fig. 2.2C. The difference between the DLS measurements and the calculated diameter from the TEM images was likely caused by both the folic acid shell and aggregation in the

sample. The functionalization of folic acid to the CuS NPs is critical for their use in tagging ovarian cancer cells. The particles were analyzed to determine successful folic acid functionalization through MALDI-TOF. A saturated solution of folic acid in water was used to generate the positive control mass spectra shown in Figure 2.3B. Protonation of the folic acid (441.40 Da) resulted in a 2 Da increase corresponding to the most abundant peak recorded, 443.32 Da. FA-CuS NPs were subsequently analyzed to produce the spectra shown in Figure 2.3C.

Folic acid was successfully identified in the NPs, producing two peaks at 441.17 and 443.17 Da. Mass shifts corresponding to the addition of copper atoms could be identified in the spectra. Masses 504.25 and 506.25 correspond to folic acid (441.17 or 443.17 Da). The addition of a single copper atom (63.55 Da) and mass 588.17 is assumed to be folic acid plus the addition of two copper atoms. Results from the MALDI-TOF analysis of FA-CuS NPs suggest that the folic acid was bound to the CuS NPs.

2.3.2 In-Vitro Uptake of FA-CuS NPs

To investigate the cellular uptake of our FA-CuS NPs, fluorescently tagged NPs were incubated with SKOV-3 cells and then imaged using fluorescence microscopy. The folate receptor, which is often overexpressed on the surface of ovarian cancer cells, has remained an ideal target for NPs and other PA contrast agents.[131,79] In this study, SKOV-3 cells were selected due to the high expression of the folate receptor on their outer membrane.[120] FA-CuS NP uptake was measured by fluorescence as com-

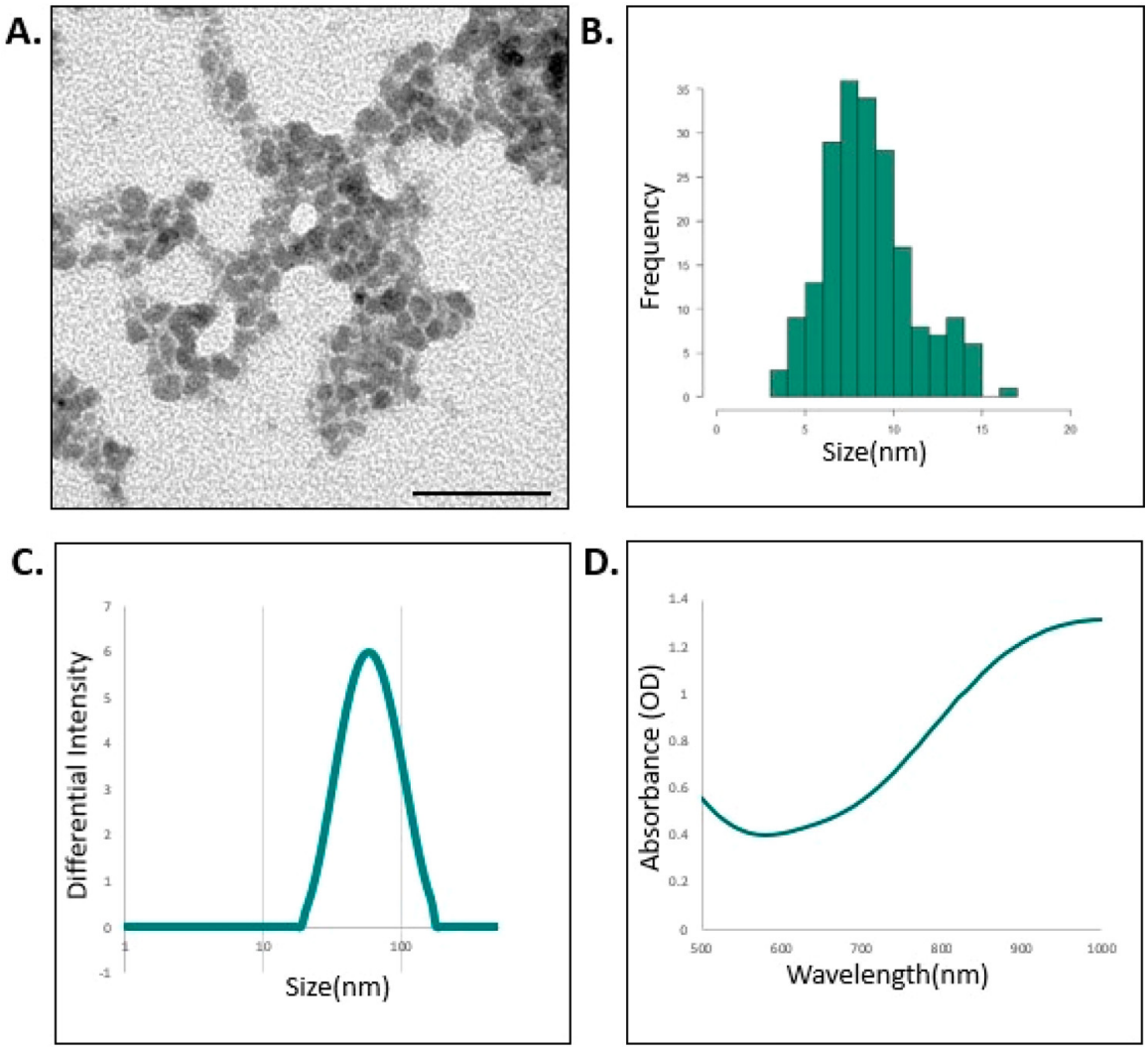

Figure 2.2: (A) Representative TEM Image of FA-CuS NPs. Scale Bar Is 50 nm. (B) Size Distribution of FA-CuS NPs. (C) Representative DLS Intensity Distribution of FA-CuS NPs. (D) Absorbance Curve of FA-CuS NPs.

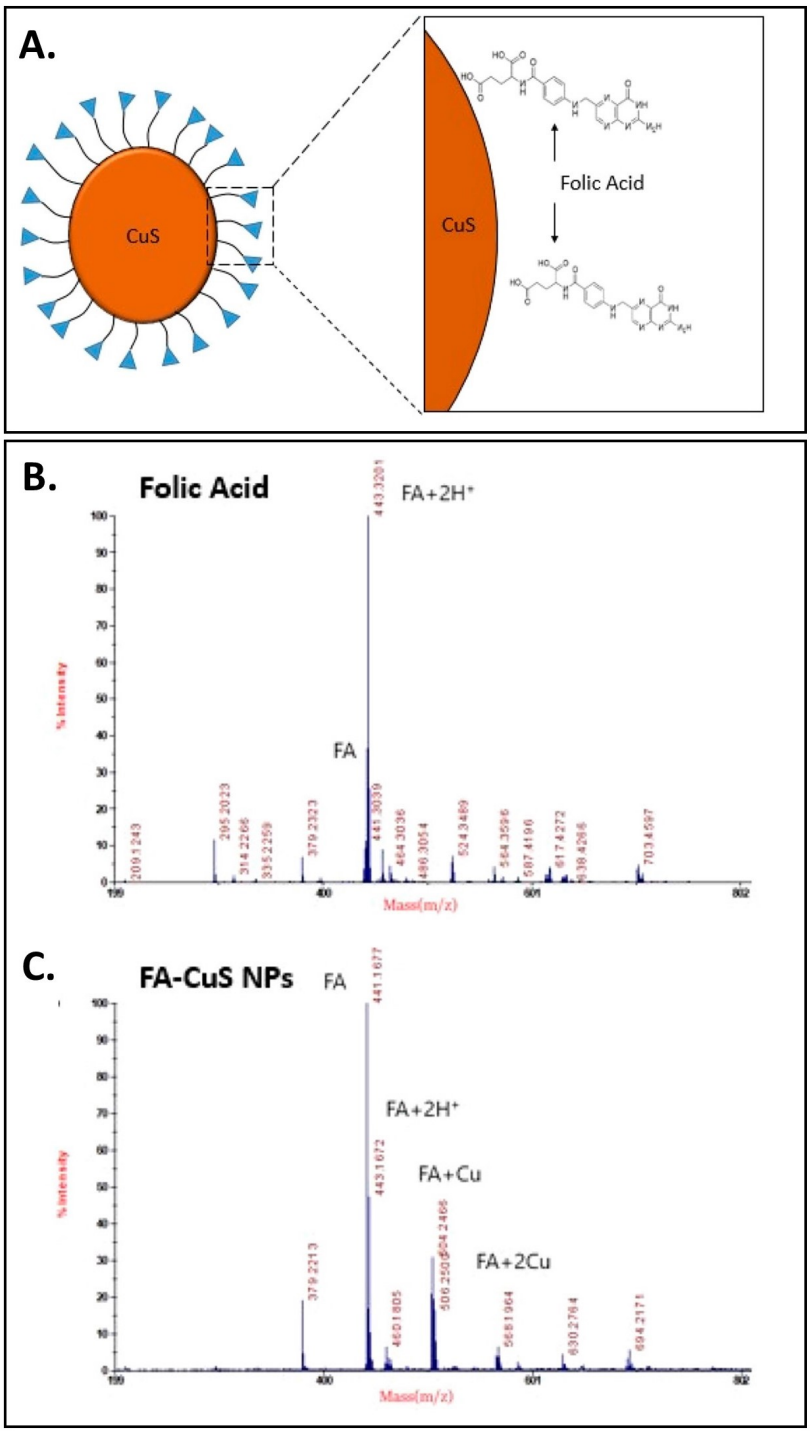

Figure 2.3: (A) FA-CuS NP Capping Strategy. (B) MALDI Spectra from Folic Acid. (C) MALDI Spectra of the FA-CuS NPs.

pared to the negative control. SKOV-3 cells incubated with the fluorescently tagged NPs displayed fluorescent intensity throughout the cell following the uptake of the FA-CuS NPs, as seen in Fig. 2.4. NP uptake was observed for all the concentrations of FA-CuS NPs that were tested (results shown only for the 400 μg/mL concentration). By fluorescently labeling our FA-CuS NPs, we were able detect the presence of our FA-CuS NPs throughout the cytoplasm. The FA-CuS NPs were detected at concentrations as low as 100 μg/mL. This observation suggests that the particles are taken up into SKOV-3 ovarian cells and can be utilized to detect these cells using our PAFC system

2.3.3 Photoacoustic Detection of Cells in Flow

To the best of the authors' knowledge this is the first time ovarian CTCs have been detected by PA in a flow system. Our PA flow system consisted of dual syringe pumps simultaneously pumping the sample and air through the system. This created two-phase flow, with alternating sample and air passing through the flow chamber where it was irradiated by NIR light and the PA signal was recorded. Each sample that passed the path of the laser was approximately 1 μL in volume, containing on average one cell per sample. To test the ability of our setup to distinguish NP-tagged SKOV-3 cells, four samples were evaluated in our PA flow system: (1) PBS, (2) 100 μg/ mL FA-CuS NPs in PBS, (3) SKOV-3 cells tagged with FACuS NPs in PBS, and (4) SKOV-3 cells alone in PBS at a concentration of 1000 cells per/mL. To ensure that the samples moved uninterrupted through the flow system, 2% TWEEN was added

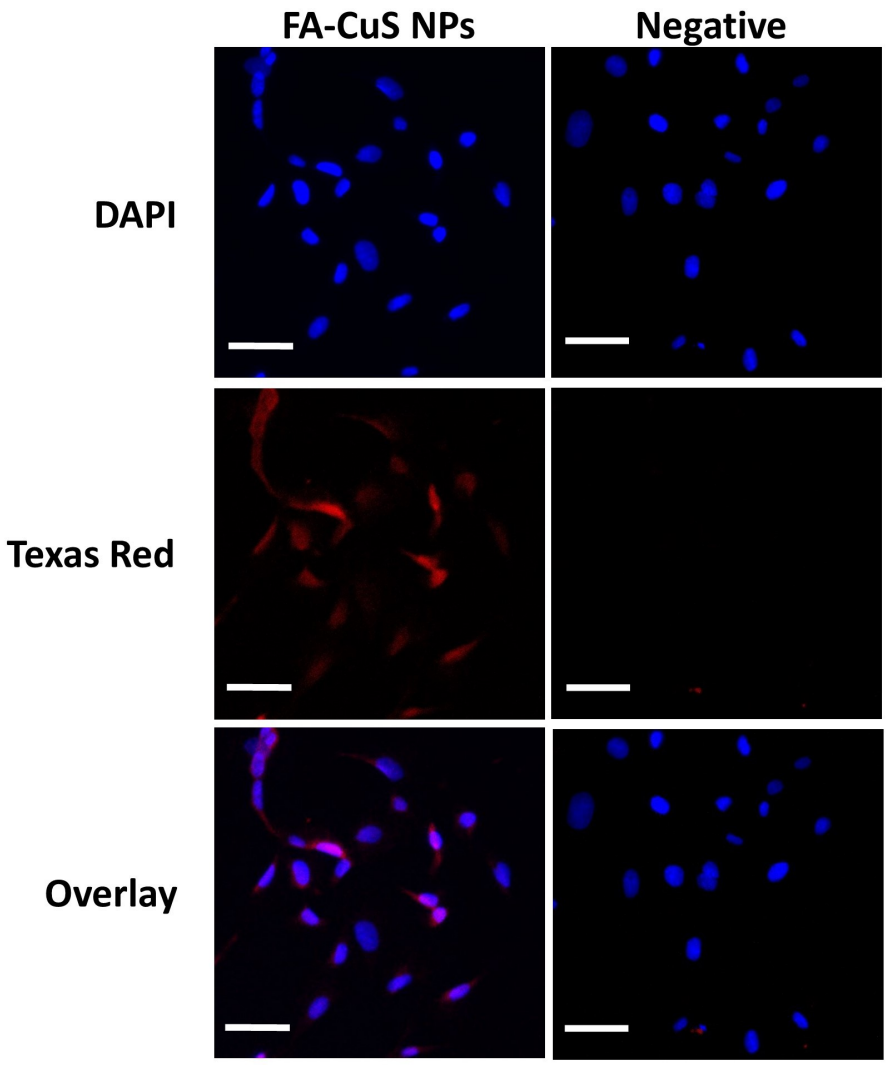

Figure 2.4: Representative Fluorescence Images of SKOV-3 Cells Incubated with and Without 400 μg/mL Fluorescently Tagged FA-CuS NPs for 2 H. Scale Bar Is 50 μm. Cell Nuclei Were Stained with DAPI.

to each of the samples. Higher concentrations of cells were tested; however, this led to inconsistent results. The authors attribute this to clogging of the system at high concentrations. For each of the sample conditions, 3 runs lasting 500 acquisitions were recorded. Recordings of the laser and the passage of samples through the flow chamber were collected using a microscope-mounted CCD camera (Thorlabs, Austin TX). For the cells with NPs, cells alone, PBS, and NPs alone, the amounts of total acquisitions examined were 203, 150, 160, and 131, respectively.

2.3.4 Data Analysis of Photoacoustic Detection of Cells in Flow

For each acquisition of the PA signal, a Hilbert transform was applied. An analytic signal was then created by combining the data with its own Hilbert transform. The magnitude of the analytic signal was subsequently calculated and integrated to measure the total signal resulting from each acquisition. These values were taken for all samples within each test group. Representative image reconstructions of the PBS and the FA-CuS NPs signals are presented in Fig. 2.6.

The concentration of 100 μg/mL of FA-CuS NPs produced a significant PA signal from stimulation by 1053 nm with a pulse-energy of $\sim$8 mJ, thus indicating sufficient energy for PA signal generation. The integrated signals were averaged and compared utilizing a Welch's t test. Representative raw and Hilbert transformed signals are presented in Fig. 2.7.

At a concentration of 1000 cells/mL, the results showed a significantly higher mean signal in the group of cells that were tagged with FA-CuS NPs ($p < 0.05$) than

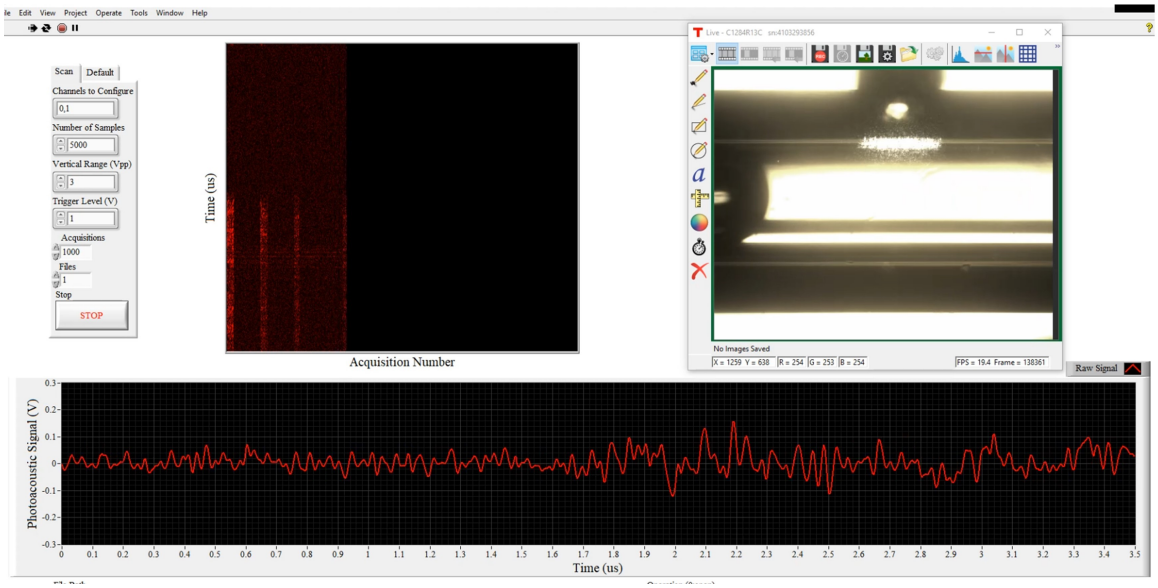

Figure 2.5: Image Depicting the Flow System Scanning CuS Nanoparticles at a Concentration of 100 μg/mL.

the same concentration of cells that had not been incubated with NPs. In addition, when untreated cells were analyzed in the system, the PA signal was not significantly different than that of PBS alone ($p < 0.05$). The box plots of these signals are displayed in Fig. 2.8. The successful identification of ovarian CTCs in flow provides insights into future *in vitro* and *in vivo* applications of PAFC. The concentration of 100 μg/mL FA-CuS NPs produced a significant PA signal. Our results clearly indicate the capacity to detect ovarian CTCs by utilizing FA-CuS NPs in our custom flow system.

2.4 Conclusion

In this study, we have developed a novel system for the PA detection of ovarian CTCs in flow utilizing FA-CuS NPs. Through the development of a custom PA flow

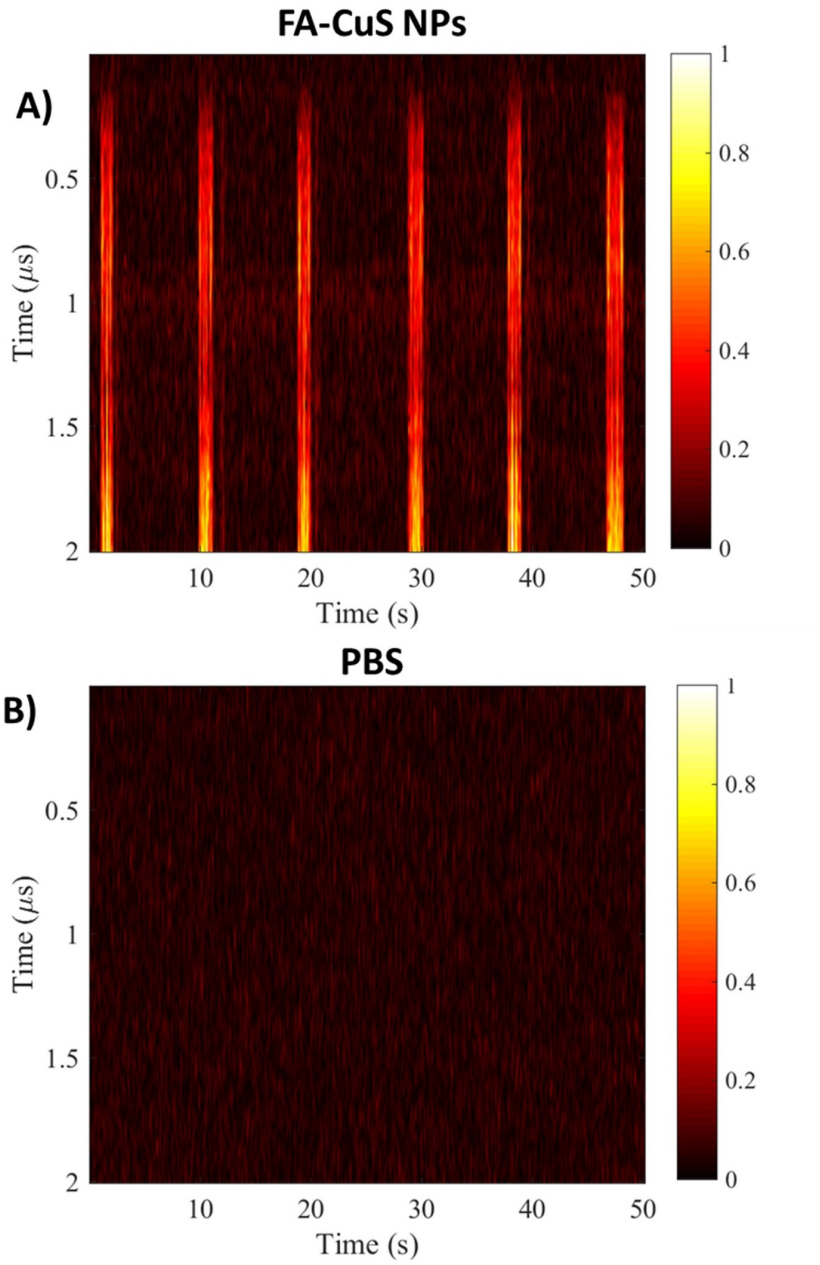

Figure 2.6: Photoacoustic Image Reconstructions of (A) 100 μg/mL of FA-CuS NPs in 2% Tween and PBS and (B) PBS with 2% Tween in the PAFC. The Alternating FA-CuS NP Sample Generates a Very Strong Photoacoustic Signal

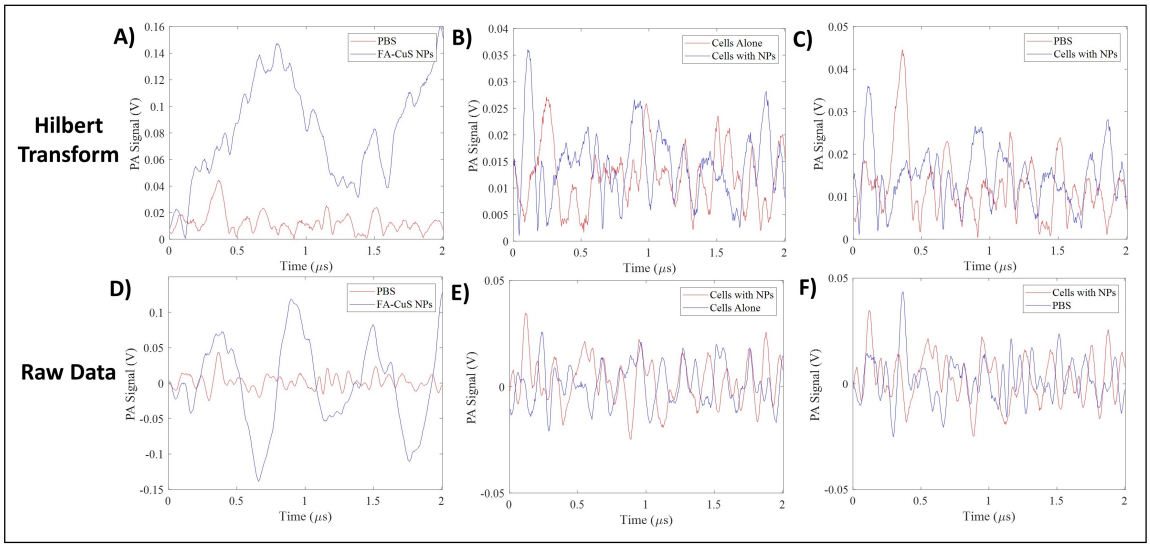

Figure 2.7: (A) Representative Raw Data Signal from FA-CuS NPs and PBS and (D) the Hilbert Transform of the Data. (B) Representative Raw Data Signal from Cells with NPs and Cells Alone and (E) Corresponding Hilbert Transform. (C) Representative Raw Data Signal from Cells with NPs and PBS and (F) Corresponding Hilbert Transform.

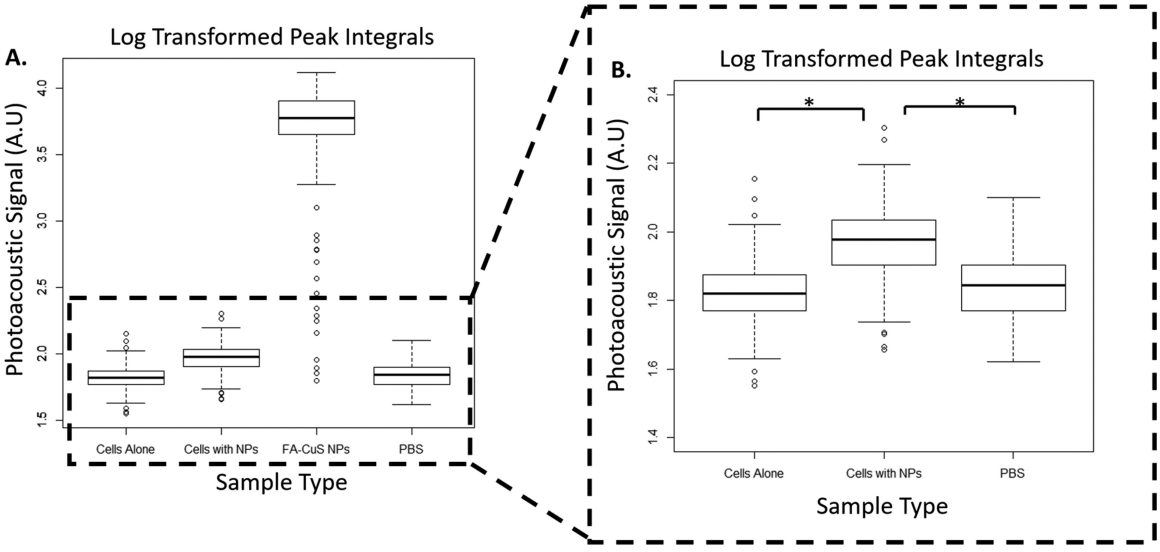

Figure 2.8: (A) Log Transformed Peak Integrals of Cells Alone, Cells with NPs, FA-CuS NPs, and PBS. (B) Breakout Box Plot of Log Transformed Peak Integrals from Cells Alone, Cells with NPs, and PBS.

setup, we have detected down to 1 cell/sample using FA-CuS NPs. These results suggest the ability of our system to identify ovarian CTCs at physiologically relevant concentrations. By functionalizing our NP system with folic acid, the NPs were specifically designed to be taken up by ovarian cancer cells. Fluorescence microscopy indicated significant uptake of FA-CuS NPs by SKOV-3 cells. We have developed a system that has produced high intensity PA signal for the noninvasive detection of ovarian CTCs. This study enables the clinical application of CTCs to detect early stages of metastasis in ovarian cancer. Further studies will provide a better understanding of the level of specificity of this technique for use in clinical applications

Chapter 3

IMAGING NIR PROTEINS IN CELLS *IN VITRO* UTILIZING A CUSTOM PHOTOACOUSTIC MICROSCOPY (PAM) SETUP

3.1 Introduction

Imaging neuronal subtypes at increased depth in the mammalian brain is critical for understanding neurological processes. Microscopy techniques such as widefield, structured illumination, confocal, two-photon, and light-sheet have been widely applied in neuroscience applications. However, the imaging depth of these optics-based methods is constrained by the scattering of light in tissues.[152] To address these issues, multi-photon microscopy has emerged as an effective technique for high-resolution imaging deep in biological samples.[63]

Though multi-photon microscopy has expanded the capabilities of biological imaging, this technique is still limited to a depth of 1 mm in tissues.[5,147] In addition to advances in optics, new fluorophores have been developed for fluorescence microscopy that absorb NIR light, further expanding the depth of these traditional microscopy techniques.[163] However, many of these NIR fluorophores still use purely optics-based approaches for manipulating and imaging cells, limiting their effectiveness. Further research is necessary to develop new methods that increase the imaging depth past the current limit of traditional microscopy.

Combining genetic labeling strategies with technologies capable of imaging at increased depth beyond the cortical surface will significantly expand the type and variety of cells that neuroscientists can investigate. As a first step toward this goal, we utilize iRFPs combined with PAM to label and detect B35 neuroblastoma cells. PAM relies on the PA effect to generate contrast for imaging.[50] Because PAM utilizes ultrasound to detect signals, these PA systems penetrate more deeply into tissues than conventional microscopy methods.[152] Furthermore, using PAM in combination with NIR contrast agents can further extend the depth at which these techniques can be employed in the field of neuroscience. PA contrast agents synthesized from various materials have been developed to extend the depth of imaging of PA beyond its current capabilities.[81,74,54,59] Among these materials, a new class of NIR genetically encoded fluorophores, iRFPs, have been expressed in specific cell types and utilized as contrast agents for PA and fluorescence studies.[29] Recent studies have shown the potential for PAM to image cells at greater depths when combined with these NIR fluorophores.[59,29] None of these studies have utilized iRFP with PAM for neuron-specific detection *in vitro*.

In this study, we construct a PAM system to detect genetically encoded iRFP contrast agents in neuronal cells. For the first time, we demonstrate the ability to detect genetically encoded contrast agents in neuronal subtypes utilizing PA. This research opens new avenues for characterizing a variety of genetically encoded NIR contrast agents in neuronal cells *in vitro* using PA for the advancement of neuroscience.

3.2 Materials and Methods

3.2.1 Cell Culture and Transfection

The B35 cell line (rat neuroblastoma) was purchased from ATCC (CRL-2754, American Type Culture Collection). B35 cells were cultured in Dulbecco's Modified Eagle Medium (DMEM) supplemented with 10% fetal bovine serum (FBS), 100 U/mL penicillin, and 100 µg/mL streptomycin and were maintained at 37°C in a humidified 5% CO2 incubator. For cell culture transfection, the plasmid piRFP was utilized to create a monoclonal cell line (piRFP was a gift from Vladislav Verkhusha (Addgene plasmid 31857; http://n2t.net/addgene:31857; RRID:Addgene_31857).[30] Plasmid DNA was isolated utilizing a Plasmid Mini Kit (Qiagen). The DNA was then analyzed by nanodrop and gel electrophoresis. The plasmid DNA was linearized using an ApaI restriction enzyme, and B35 neuroblastoma cells were transfected using lipofectamine 2000 (Thermo Fisher Scientific) according to the manufacturer's instructions. Transfected cells were selected by G418 Sulfate for seven days at a 400 µg/mL concentration and were further grown and expanded in media with a G418 concentration of 200 µg /mL. Monoclonal iRFP cell lines were isolated by transferring single cells from the polyclonal line into individual wells of a 96 well plate. The resulting monoclonal lines were then evaluated by fluorescence microscopy and flow cytometry (ThermoFisher Attune NxT - Cell Analyzer). The cell line with the brightest median and mean fluorescence values was used in subsequent experiments.

3.2.2 PAM System Architecture

The NIR-PAM system is depicted as a schematic in Fig. 3.1. The laser source for the system is a tunable LS2134-LT40 Nd:YAG/Ti:sapphire Nanosecond Pulsed Laser (Symphotic TII Corporation). The laser has an excitation light with a full width half maximum (FWHM) of 12 to 15 ns at a pulse repetition rate of 10 Hz with specific wavelength operation at 532 and 1064 nm and tunable wavelength from 690 to 1000 nm. The wavelength was tuned to 700 nm to excite iRFP proteins. The laser first passes through a neutral density filter and is guided by a mirror through a 1 mm aperture. A portion of the laser light passes through the mirror and strikes a reference transducer to time the firing of the laser. It is then focused through a plano-convex lens (ThorLabs, LB1757-B) and further collimated by another plano-convex lens (ThorLabs, LA1229-AB) to a diameter of 6 mm. The light then passes through a neutral density filter and a beam splitter (Thorlabs, BS025). The collimated light is directed to a 40x objective lens (Motic, 1101001703112), and focused on a sample in a custom 3D printed water tank Fig. 3.1B. The beam splitter allows light coming back from the PAM system to be viewed on an in-line camera. The tank is connected to a micromanipulator (Patchstar, Scientifica) which allows for the manipulation and scanning of samples. The tank is filled with PBS, and a focused ultrasound transducer is confocally aligned above the focal point of the objective lens. PA signals generated by the laser are detected by a focused ultrasound transducer, with a center frequency of 25 MHz (Olympus, V324-N-SU). Signals detected by the

focused ultrasound transducer are sent to two amplifiers (Mini-Circuits, ZFL-500LN-BNC+), and signals detected by the reference transducer are sent to the ultrasound pulser/receiver (5077PR Square Wave pulser/receiver, Olympus Inc.). Amplification is performed through a 59-dB gain and filtered with a 1 to 10-MHz bandpass filter. A multipurpose reconfigurable oscilloscope (NI PXIe-5170R, National Instruments Corporation) is used for data acquisition and equipped with a built-in FPGA. Multipurpose, programmable function input/output lines built into the FPGA are used for custom triggering and synchronization of the PAM system.

3.2.3 Cell Preparation for Fluorescence and PAM Evaluation

Cells for fluorescence microscopy were seeded on glass coverslips in a 24 well plate at a density of 0.071 x 10^6. Approximately 24 hours after being seeded, cells were washed with pre-warmed PBS, incubated with 4% PFA in PBS for 15 minutes, incubated with 0.1% Triton-X for 5 minutes, and washed three times with PBS in 5-minute increments. Cells were then stained with DAPI and Alexa Fluor 568 Phalloidin for 5 minutes. The stains were removed, and the cells were washed three times with PBS and mounted on coverslips using Prolong Diamond Antifade. The cells were imaged by Leica SP8 White Light Laser Confocal Microscope housed in the Regenerative Medicine and Bioimaging Facility at Arizona State University that was acquired by the NIH SIG award 1 S10 OD023691-01. To prepare cells for PAM experiments, both monoclonal iRFP cells and non-transfected B35 cells were grown to a confluency of approximately 80-90%. The cells were then trypsinized with 0.05%

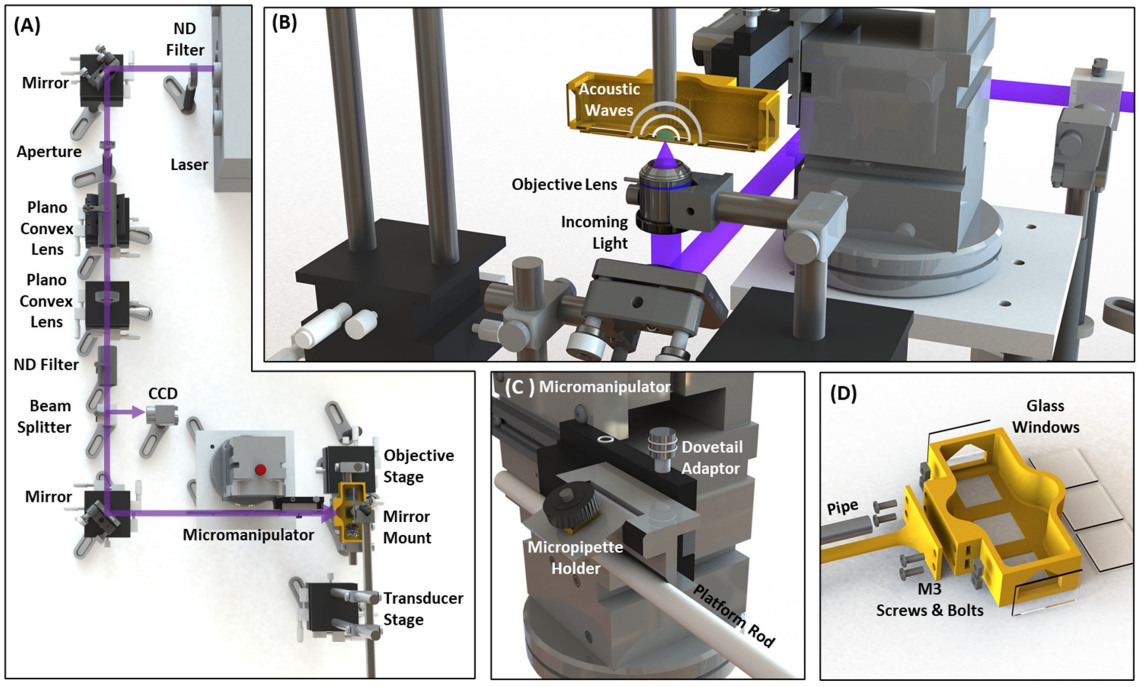

Figure 3.1: (A) System Architecture. Excitation Light from a 700 nm Tunable Laser Is Spatially Filtered and Directed to an Objective Lens at the Photoacoustic Microscopy (PAM) Setup. An In-line Beam Splitter Samples Some of the Light Returning from the PAM Setup to Image the Sample. (B) Light Is Directed onto the Sample Within the Custom PAM Sample Tank from a 40x Objective Lens, and a Confocally Aligned Focused Ultrasound Transducer Detects Photoacoustic Signals Produced by the Sample. (C) a Platform Rod Connects the Micromanipulator to the Custom PAM Tank, Allowing for Precise Sample Manipulation. (D) Exploded View of the Custom 3D Printed Sample Tank

trypsin with EDTA, centrifuged at 123 x G for 6 minutes, and diluted in PBS to the desired concentration 0.4-3.2 $*10^5$ cells/µL. The cell solution was then mixed with a 1:1 mixture of 2% low melt agarose in PBS to form a 1% agarose solution with a final concentration of 0.2-1.6 $*10^5$ cells/µL. Finally, 25 µL of the solution was slowly dispensed on a piece of parafilm using a 200 µL micropipette to produce cylindrical beads. After the gels had solidified, both non-transfected and transfected cells were evaluated by PAM and imaged by fluorescence in a c400 Azure gel imager. The

PAM experiments evaluated three independent transfected and non-transfected cell populations in agarose gels.

3.3 Results and Discussion

3.3.1 Generation and Evaluation of Monoclonal iRFP Cell Lines

This work represents a step forward in detecting neuronal cells utilizing PA. Combining advanced genetic techniques with PA technologies has the potential to push the boundaries of what is possible in neuroscience. IRFP has been used for PA to expand the depth of imaging in tissues.[29] However, to the best of the authors' knowledge, these technologies have never been utilized to identify neuronal cells. To unite these two research fields, we sought to validate our PAM system by detecting iRFP *in vitro* in transfected B35 neuroblastoma cells.

An iRFP cell line was generated to evaluate the ability of our PAM system to detect iRFP in neuronal cells. A monoclonal cell line was selected to provide more consistent expression of iRFP than a polyclonal line. The method used for isolating plasmid DNA and transfecting B35 cells is presented in Fig. 3.2A. Plasmid DNA was isolated and further characterized by gel electrophoresis and nanodrop (Fig. 3.3), showing successful isolation of high-quality plasmid DNA. After cellular transfection and further isolation of monoclonal cell lines, they were evaluated by flow cytometry (Fig. 3.4) to identify the cell line with the highest iRFP expression for future PAM experiments. The cell line labeled F8 was selected because it had the highest mean

and median iRFP fluorescence. We then performed confocal fluorescence microscopy which showed iRFP expression across the cell (Fig. 3.2B) and confirmed the results obtained from flow cytometry. These experiments demonstrated that we had isolated a monoclonal line with consistent iRFP expression that could be utilized for further PAM experiments.

3.3.2 Evaluation of iRFP cells by NIR-PAM system

After verifying iRFP expression in our neuronblastoma cell line, we sought to test the ability of our PAM system to detect iRFP in these cells. With the goal of ultimately imaging iRFP that had been transgenically expressed in brain slices, we made tissue-mimicking agarose gels to test the cells' ability to generate the PA effect in a 3D cell culture environment. We then tested the limit of detection of the PAM system. Dilutions of both transfected and non-transfected cells in 1% low melt agarose were prepared, spanning from 0.2 to 1.6 $*10^5$ cells/µL. The cell dilutions were then imaged using an Azure c400 gel imaging system and the results can be seen in Fig. 3.5A. The fluorescence from iRFP can be seen in the gels that have been transfected with iRFP and fades with decreasing cellular concentration. There is no fluorescence seen in non-transfected B35 cells. The cells were then systematically tested for their ability to generate the PA effect. The PAM system was optically focused at the center of the gel, and 4000 shots were fired. The data was then averaged to provide the total PA signal, as presented in 3.5B. This data demonstrated that our NIR-PAM system has a limit of detection of 1.6 $*10^5$ cells/µL. To confirm that our system was capable of

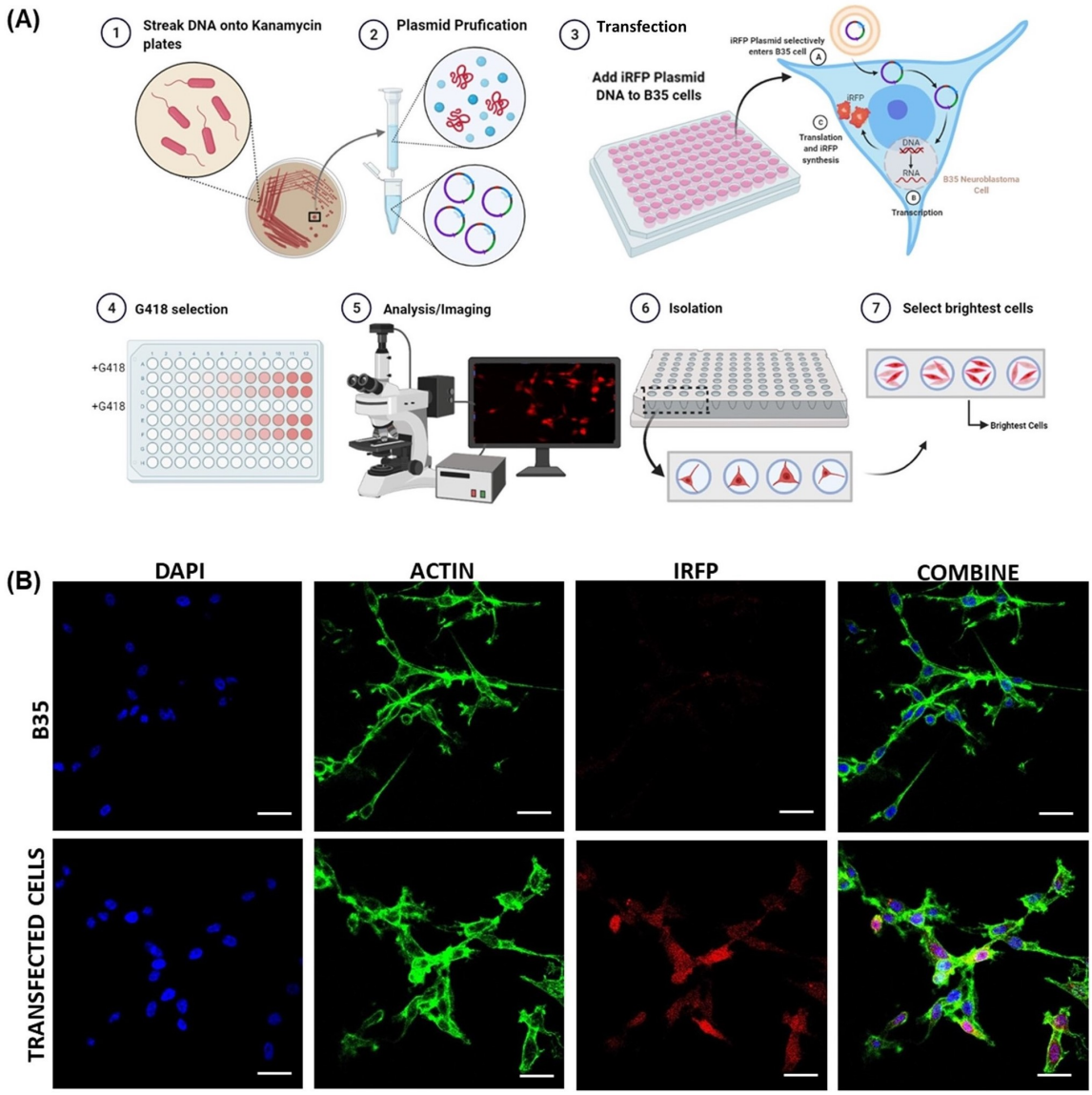

Figure 3.2: (A) Monoclonal IRFP Transfection and Isolation Process. Diagram Made with Biorender.com (B) Fluorescence Microscopy of Monoclonal Transfected IRFP Cells and Non-transfected B35 Cells. Scale Bar Is 10 Microns.

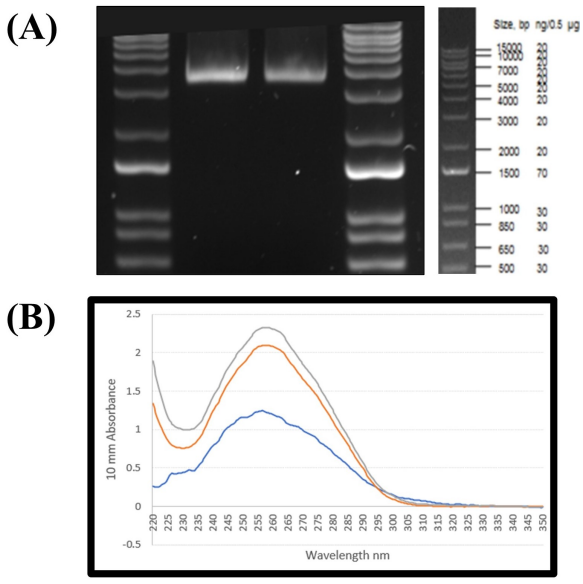

Figure 3.3: (A) Gel Electrophoresis of Isolated Plasmid DNA. (B) Nanodrop Data of Isolated IRFP Plasmid DNA.

consistently detecting iRFP in agarose gels at this concentration, three independent experiments were performed with iRFP cells at a concentration of 1.6 *10^5 cells/µL. The results of each of these independent runs can be seen in Fig. 3.6A. Results indicate that there is a clear PA signal for each run containing iRFP transfected cells vs. the non-transfected cells. In addition, we once again saw consistent fluorescence signal throughout the transfected B35 cells in agarose as compared to the negative control (Fig. 3.6B). Previous studies have examined the PA properties of iRFP in MTLN3 and Hela cells, however, to the authors' knowledge, no studies have yet explored whether this chromophore can be detected in neuronal cell culture.[29,66] These experiments confirmed the ability of the custom PAM system to detect PA signals from iRFP transfected B35 cells. In addition, and importantly, it shows the capability of iRFP to produce both fluorescent and PA contrast in our neuronal cell line. These

(A)

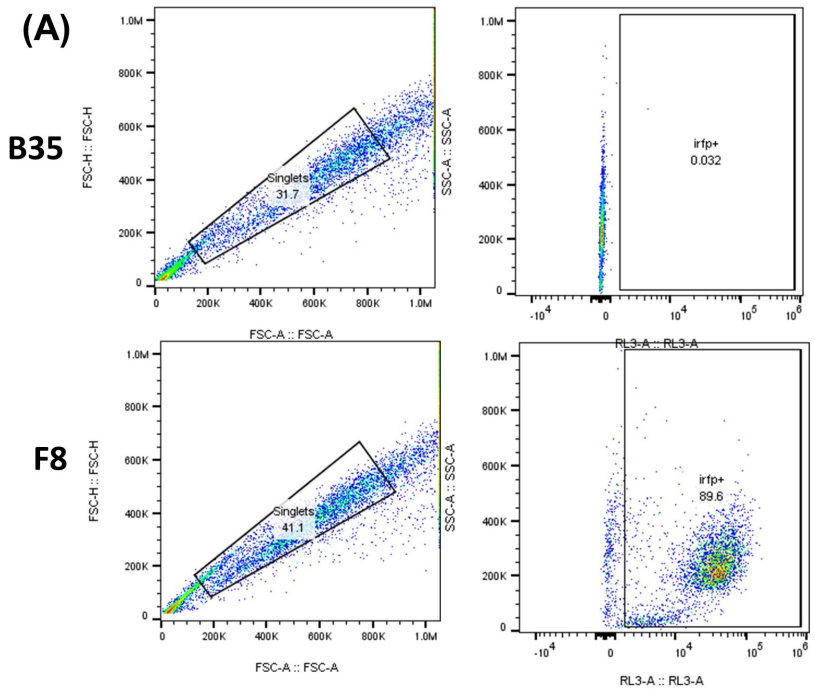

(B)

Sample	Median iRFP Signal	Mean iRFP Signal
B35	5611	5611
F8	31269	33900
B9	23978	27082
C8	24949	31581
E11	4140	16185

Figure 3.4: (A) Flow Cytometry Data from Singlet Isolation and IRFP Expression from Flow Cytometry Experiements for F8 and B35 IRFP Negative Cells. (B) Median and Mean Fluorescence Measurements of B35 Non-transfected Cells and Selected Monoclonal Cell Lines.

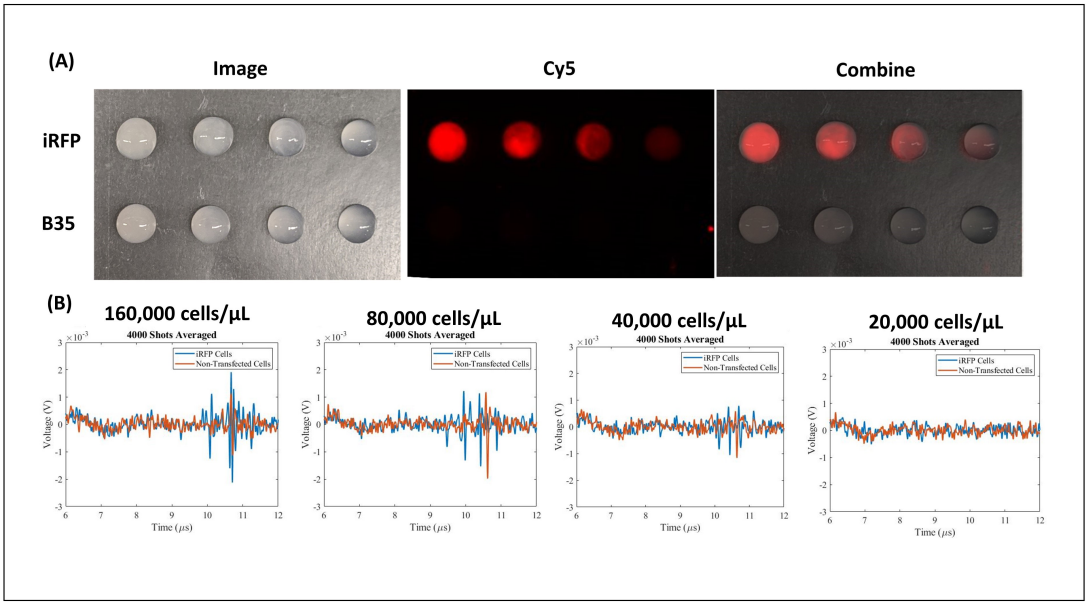

Figure 3.5: (A) Agarose Gel Dilutions of Transfected IRFP and B35 Cells. Concentrations Are 160,000-20,000 Cells/μL from Left to Right (B) Corresponding Photoacoustic Data from the PAM system.

results demonstrate that the NIR-PAM system can detect iRFP in neuronal cells and support further studies evaluating iRFP and other genetically encoded proteins *in vitro*.

3.3.3 Limitations

One limitation of this study is the large number of cells required to generate a PA effect. To solve this problem, in future studies cells will be characterized cells *in vitro* using lasers with higher pulse rates and more powerful ultrasound transducers. Although we have not yet evaluated the expression of these near-infrared proteins in single cells, we believe that the PAM system described here will be capable of characterizing a wide variety of NIR genetic probes *in vitro*. The current system is

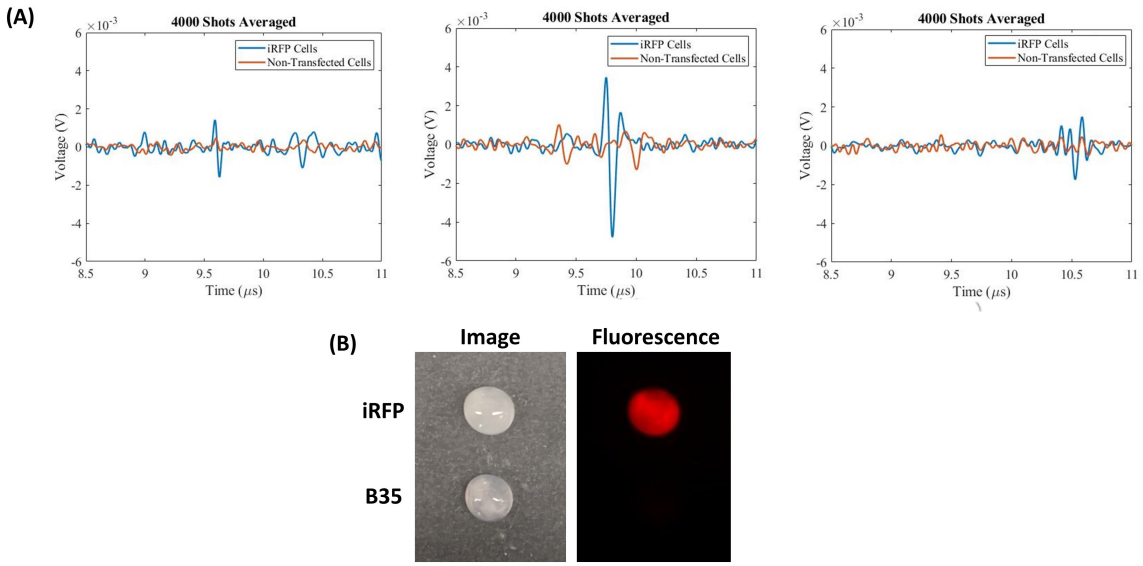

Figure 3.6: (A)Photoacoustic Data from 3 Independent Runs of IRFP Agarose Gels at a Concentration of 160,000 Cells/μl (B) Fluorescence Data from Agarose Gel Imaging.

equipped to evaluate biological samples by bright field microscopy and PA. Future studies will outfit the PAM system with fluorescent filters and a fluorescent light source to enable dual PA and fluorescence microscopy of cells. This will allow for simultaneous characterization of fluorescent and PA feedback, giving greater insights into the performance of these genetically encoded contrast agents.

3.4 Conclusion

In this study, we demonstrate, for the first time, that iRFP can be detected in neuronal cells by PA. These results demonstrate our ability to detect iRFP in neuronal cells *in vitro* and support the further use of this system to detect iRFPs in mammalian brain slices. In addition, this PAM system has the capability to examine a variety of NIR probes including optogenetic labels, and calcium and voltage indicators.[107,114,104]

This system could also be utilized to characterize the PA response of genetically encoded probes in primary cells isolated from brain tissues. This study represents a first step towards utilizing PAM to characterize protein expression in neuronal cell culture *in vitro*.

Chapter 4

DETECTION OF IRFP IN TRANSGENIC MICE

4.1 Introduction

Current imaging strategies for detecting neurons *in vivo* lack the depth of penetration and specificity needed to target deep-brain neuronal subpopulations. Neuroscientists have been limited in their ability to image deeply in the brain at high resolution using traditional microscopy and imaging methods.[10] Researchers have attempted to overcome this limited imaging depth through the advancement of light microscopy, endoscopy approaches, and the engineering of NIR probes.[63,163,127,9] Despite these technological advancements, there are still limitations to the depth that genetically modified neurons and fluorescent probes can be imaged.

Approaches that are commonly utilized for imaging genetic reporters in the brain include confocal, multiphoton, and light-sheet microscopy. Though these imaging modalities have good resolution, they fail to detect neurons at increased depths in the brain due to the optical absorption of light in tissues.[152] In addition, endoscopy methods have greatly extended the reach of optical imaging in neuroscience by placing waveguides deep into the brain.[127,19] Although these endoscopy methods are very effective, they can cause damage to tissue, and their effects on experimental conditions must be considered. Overall, new strategies for the imaging of genetically encoded

contrast agents need to be evaluated to expand the scope of neuroscience research in the brain.

PA imaging has emerged as a noninvasive imaging modality that has extended penetration depth in tissues over purely optics-based methods.[132] PA technologies have been used extensively to image structures in the brain, with the majority of studies centered on imaging brain vasculature.[10] Recent studies have shown the capability of PA signals to travel through the skull and measure hemodynamics across the brain in mouse models.[10,162] Though genetic reporters have been used in combination with PA brain research, they have never been, to the best of the author's knowledge, utilized to visualize or detect neurons within the brain directly using iRFPs.

IRFPs have been successfully used as contrast agents in PA research to expand imaging penetration using NIR light.[29,59] These studies successfully imaged iRFP at depths of up to 4 mm in tissues utilizing PAM.[29] However, previous PA studies have only utilized transfected populations of cells injected into animals, failing to characterize cellular subtypes in tissues. To label specific neuronal subpopulations, neuroscientists have used iRFP with Cre-Lox recombination to preferentially express iRFP in dopaminergic neurons in transgenic mice and rats.[107] In these studies, iRFP was found not to affect neuronal firing and extend the depth of imaging of neurons.[107] This makes iRFP an ideal contrast agent for use in combination with optogenetics and PA imaging to enable deep brain imaging *in vivo*. Leveraging these advanced genetic strategies combined with PA technology, we aim to expand the scope of specific

neuronal imaging in the brain.

This study utilizes PAM in combination with iRFP expressed using Cre-Lox recombination to detect neuronal cells in brain slices. For the first time, this study utilizes Cre-Lox recombination to detect neurons using PAM, providing a new path forward for the PA detection of neuronal subtypes in the brain.

4.2 Materials and Methods:

4.2.1 PAM System Architecture

For information regarding the construction of the PAM system please refer to Chapter 3 of this dissertation.

4.2.2 Animal Usage Ethics statement

All experimental designs using mice were reviewed and approved by the Institutional Animal Care and Usage Committees at Arizona State University (Protocol#19-1697R) and conformed to all regulatory standards. All mice examined in this study were euthanized via CO2 inhalation or fully anesthetized with ketamine/xylazine prior to intracardial perfusion as described in the AVMA Guidelines on Euthanasia.

4.2.3 Mice and Genotyping:

In this study, $DAT^{IREScre}$ ($DAT^{IREScre}$ B6.SJL-$Slc6a3^{tm1.1(cre)Bkmn}$/J) heterogenous and wild-type mice were obtained from Jackson Labs (JAX Stock 006660). Mice were housed under standard laboratory conditions with *ad libitum* access to food

and water on a 14-hour light/10-hour dark cycle in vivaria at ASU. For PCR genotyping, we utilized a primer set to amplify a 560bp fragment of the cre allele (Forward (5'-3'): GCTAAACATGCTTCATCGTCGG, Reverse (5'-3'): GATCTCCGGTATTGAAACTCCAGC) from genomic DNA samples. We also used a 500bp wild-type actin primer as a control (Forward (5'-3'): CAAATGTTGCTTGTCTGGTG, Reverse (5'-3'): GTCAGTCGAGTGCACAGTTT).

4.2.4 ICV Injections and Brain Preparation

The AAV used in this study, AAV1-EF1a-DIO-Nuc-iRFP, was a gift from Dr. Brandon Harvey at the National Institute on Drug Abuse. Intracerebroventricular (ICV) injections of AAV into P0 neonatal mice were performed as previously described with minor modifications.[56] A 10 μl injection syringe (Hamilton) with a 32 G needle (Hamilton, Point Style 4, 10 mm, 12°) was inserted 3 mm into the lateral ventricle of cryoanesthesized mice. Two microliters of AAV diluted with sterile phosphate-buffered saline (AAV1-EF1a-DIO-Nuc-iRFP, 9.9E10) were injected into each lateral ventricle. Following the injection, the pups were placed on a heating pad until their body temperature and skin color returned to normal and they had recovered movement. The injected pups were then returned to their home cage. Three to four weeks after injection, the mice were intracardially perfused with ice-cold PBS and 4% Paraformaldehyde in PBS. Following perfusion, brains were extracted and postfixed in 4% PFA in PBS at 4°C overnight. The brains were then incubated in a sucrose gradient of 15% followed by 30% sucrose over three days at 4°C. Brains were

then flash-frozen in ethanol on dry ice in OCT compound and stored at -80°C.

4.2.5 Brain Slice Preparation for IHC and PAM

Fifty-micron coronal sections were obtained by cryostat (ThermoScientific CryoStar NX70) in cold PBS. The sections were kept at 4°C in PBS until scanned by the PAM system or stained for immunohistochemistry (IHC). For IHC the cells were permeabilized in .01% Triton X in PBS for 30 minutes and then blocked in a solution containing 5% normal goat serum and .01% Triton-X in PBS for 1 hour. The sections were then incubated with primary antibodies in blocking solution overnight. The primary antibodies utilized in this study were: rabbit anti-tyrosine hydroxylase (MAB152,1:1000) and mouse anti-Cre (MAB3120, 1:1000). The brain slices were washed three times with PBS and incubated in blocking solution with fluorescently conjugated secondary antibodies and DAPI overnight. The secondary antibodies utilized in this study were Alexafluor 488 Goat anti-rabbit (ab150077, 1:500) and Alexfluor 568 goat anti-mouse (A-11004, 1:500). After incubation with the secondary antibodies, the brain sections were washed three times with PBS and mounted with Promount diamond antifade. After curing at room temperature for at least 24 hours, slides were kept at 4°C and were sealed with VALAP for long-term storage.

4.2.6 Imaging and Image Processing

Slides were imaged on a Leica SP8 White Light Laser Confocal Microscope housed in the Regenerative Medicine and Bioimaging Facility at Arizona State University

and was acquired by the NIH SIG award 1 S10 OD023691-01. Positive and negative controls were cryosectioned, stained, mounted, and imaged by fluorescence microscopy and evaluated by PAM in parallel. For each IHC experimental condition that was examined, three positive and three negative brain slices were evaluated. Within each slice, three non-overlapping sections containing tyrosine hydroxylase were imaged 15 µm from the brain slice surface at 40x magnification. Slices that were evaluated by PAM were stored at 4°C in PBS after analysis and mounted with ProMount diamond antifade. They were then tile scanned at 20x magnification to identify expression of iRFP. The brightness and contrast of images were adjusted using ImageJ image processing software. All negative and positive image pairs were thresholded with the same values.

4.3 Results and Discussion

4.3.1 Expression of iRFP in Dopaminergic Cells in Transgenic Mice

To test whether our system could detect neuronal cell types labeled by AAV vectors, we used an AAV1-EF1a-DIO-Nuc-iRFP. This AAV produces nuclear-associated iRFP in a Cre-dependent manner. In combination with DAT:Cre mice, which produce Cre-recombinase in dopaminergic neurons, we aimed to selectively express iRFP. Because iRFP has been used extensively as a reporter protein for PA imaging, this enables for the first time to the best of the author's knowledge, the detection of proteins expressed by Cre-Lox recombination using PA. An AAV with a nuclear trafficking

protein was selected to confine iRFP expression to the nucleus. This will allow neurons to be more easily differentiated, in future experiments. Utilizing this strategy, we injected DAT:Cre positive and wild-type neonatal mice with AAV1-EF1a-DIO-Nuc-IRFP. Three to four weeks later, the mice were intracardially perfused with 4% paraformaldehyde, and their brains were cryopreserved after being subjected to a sucrose gradient over 3 days. The brains were cut in pairs of negative and positive mice for IHC staining and analysis by PAM. For IHC, slices were either stained for anti-TH, which is associated with dopaminergic cells, or a combination of anti-TH and anti-Cre antibodies to show colocalization of iRFP expression with both dopaminergic neurons and Cre-recombinase.

In the successfully transfected mice, our results indicated that the expression of iRFP in the midbrain correlated with TH (Fig. 4.1). In addition, for transfected DAT:Cre positive mice, the results showed iRFP that was colocalized with Cre in the striatum, as seen in Fig. 4.2. In transfected DAT:Cre positive mice, we also saw some iRFP expression that was not correlated to dopaminergic neurons and Cre-expression outside of TH labeled dopaminergic neurons. Mice that were genotyped as DAT:Cre negative and injected with the AAV-DIO-Nuc-iRFP, showed some non-specific expression of iRFP. In addition, some DAT:Cre negative slices showed slight Cre fluorescence. This was potentially due to autofluorescence, which originated from other channels or antibody cross reactivity. (Fig. 4.3). Inconsistent labeling may have resulted from the neonatal injections and the young age of the mice at the

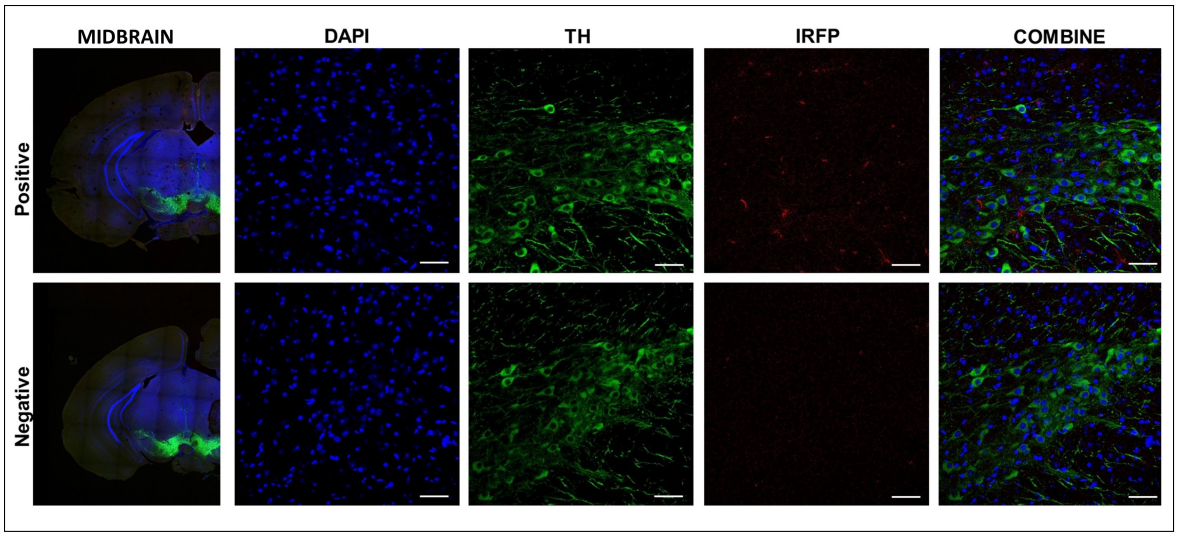

Figure 4.1: Representative Midbrain Sections of DAT:Cre Positive and Wild-type Negative Mice Injected with AAV1-EF1a-DIO-Nuc-IRFP with Corresponding Confocal Microscopy Images. An Immunohistochemistry Stain for Anti-tyrosine Hydroxylase (TH) Was Used to Indicate Dopaminergic Neurons, Showing Colocalization with IRFP. Scale Bar Is 50 Microns.

time of analysis. Future studies will further control for midbrain-directed production of iRFP through targeted midbrain injections of AAV and conditional mouse lines that can be activated with tamoxifen to have more temporal and spatial control of iRFP expression.

Confocal immunofluorescence microscopy confirmed iRFP expression in brain slices and successful characterization by the PAM system. Ultimately, we successfully produced iRFP in DAT:Cre mice in a Cre-dependent matter. This genetic expression strategy in combination with new genetic tools such as optogenetic vectors and indicators of cell activation can be used in conjunction with PA imaging to expand the studies that can be done with neuronal subtypes in the brain.

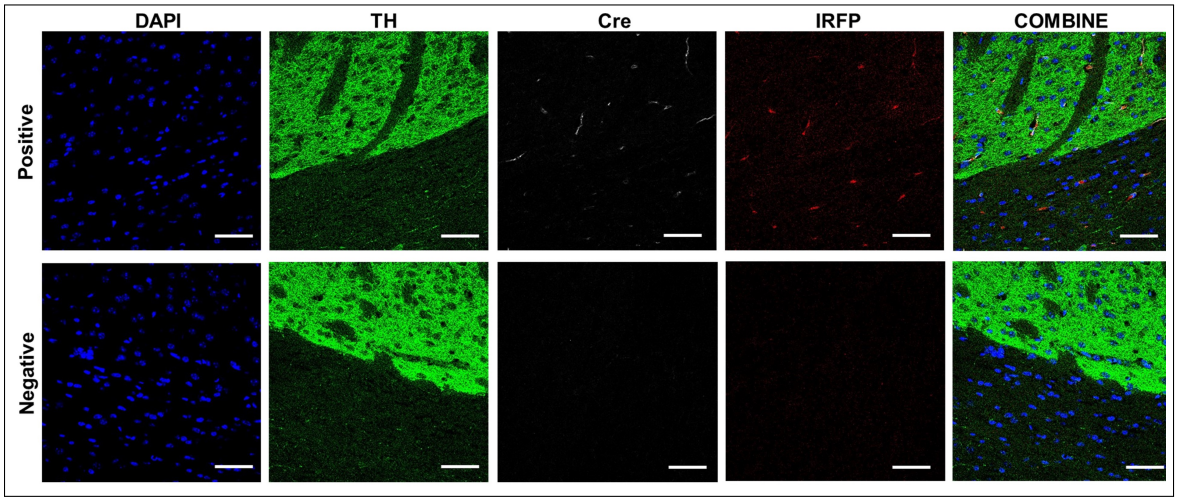

Figure 4.2: Representative Confocal Microscopy of Fixed Coronal Striatum Sections of DAT:Cre Positive and Wild-type Negative Mice Injected with AAV1-EF1a-DIO-Nuc-IRFP. Immunohistochemistry Stains for Anti-Tyrosine Hydroxylase (TH) and Anti-Cre Recombinase Were Used to Indicate Dopaminergic Neurons and Cre Expression Respectively. Both Cre and TH Show Colocalization with IRFP. Scale Bar Is 50 Microns.

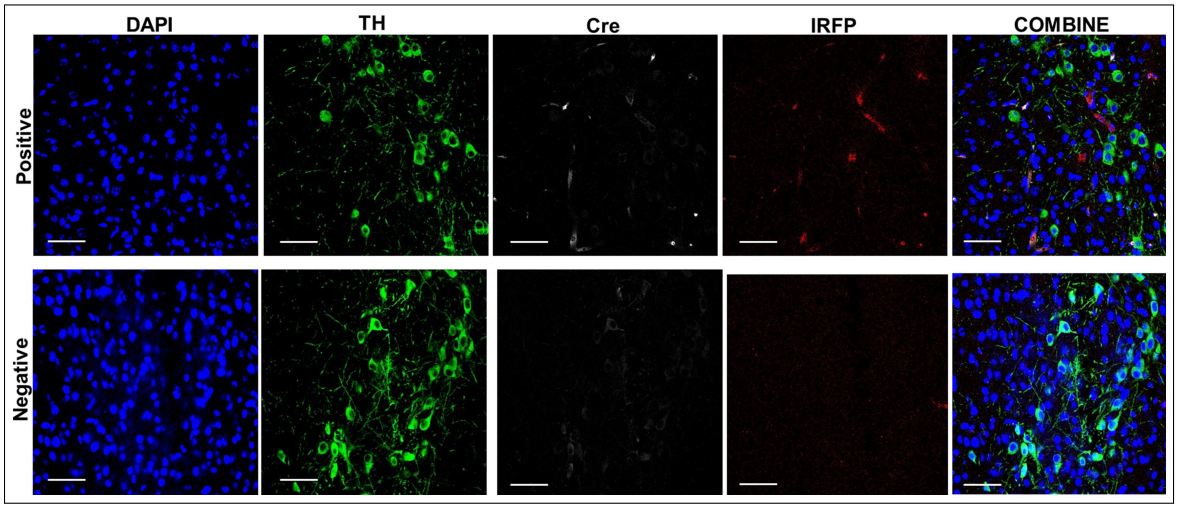

Figure 4.3: Representative Confocal Microscopy of Fixed Coronal Midbrain Sections of DAT:Cre Positive and Wild-type Negative Mice Injected with AAV1-EF1a-DIO-Nuc-IRFP. Immunohistochemistry Stains for Anti-Tyrosine Hydroxylase (TH) and Anti-Cre Recombinase Were Used to Indicate Dopaminergic Neurons and Cre Expression Respectively. Both Cre and TH Show Colocalization with IRFP. Scale Bar Is 50 Microns.

4.3.2 Evaluation of iRFP detection in iRFP brain slices by the NIR-PAM system

With the successful expression of iRFP in brain slices, and the previous experiments indicating that our PAM system could detect iRFP in neuronal cells, we tested the ability of the PAM system to detect PA signals from iRFP in brain slices. Three separate areas from two brain slices were scanned from a DAT:Cre positive and DAT:Cre negative littermate pair to determine whether differences in the PA signal were generated between iRFP negative and positive mice. Fifty-micron sections were obtained from the cryostat and were stored in PBS at 4°C. The brain slices were washed with PBS three times before scanning in the PAM setup. The sections were lowered into the bottom of the imaging tank and held down by a lead weight. The optimal z-position for acquiring data from the slices was determined by scanning a reference carbon fiber of known coordinates and finding the z-position at which the PA signal was maximized. Utilizing the in-line camera, the brain slice was brought into focus, and the z-position was adjusted to match the known optimal z-position. Three separate areas were scanned across two different sections from mice positive and negative for DAT:Cre.

Positive and negative samples were tested in alternating order to minimize the effect of fluctuating laser power on the PA signal. For each area scanned by the PAM setup, 4000 shots were acquired, and the data averaged. The resulting PA data for a positive and negative brain slice scanned in parallel are presented in (Fig. 4.4). The PA data shows the increased PA signal in the iRFP transfected brain sections versus

the negative control. Additional PA data for the second set of positive and negative brain slices are presented in Fig. 4.5. This data suggests that within brain slices, the PAM setup was able to detect cells that were expressing iRFP.

This research suggests that PA technologies can be utilized to detect protein expression in the mouse brain that is driven by Cre expression. These PA technologies could also be used in further research to look at calcium indicators, optogenetics, protein expression in neuronal subtypes with PA.[107,104] One application of this approach includes studying the expression of fos after behavioral experiments in mice.[88] A recent study examined the expression of the fos reporter using exogenous contrast generated by X-gal dye.[88] Because fos can be used as an indicator of recent neuronal activation, this study was able examine the activation of neuronal assemblies after behavioral tests using PA.[88] Future studies could be designed to examine fos expression when linked with dopaminergic cells in the midbrain by linking the expression of fos to iRFP without the need for an exogenous dye. Utilizing PA, the recent expression of neuronal subtypes could be observed at greater depths *in vivo* and in ex vivo sections.

4.3.3 Limitations

One limitation of our PAM system is using a nanosecond pulsed laser to generate the PA effect. A femtosecond laser could be applied in future studies, significantly reducing the time it takes to acquire data from samples. In addition, in future iterations of the system, fluorescent filters can be fitted inline to allow the camera to view

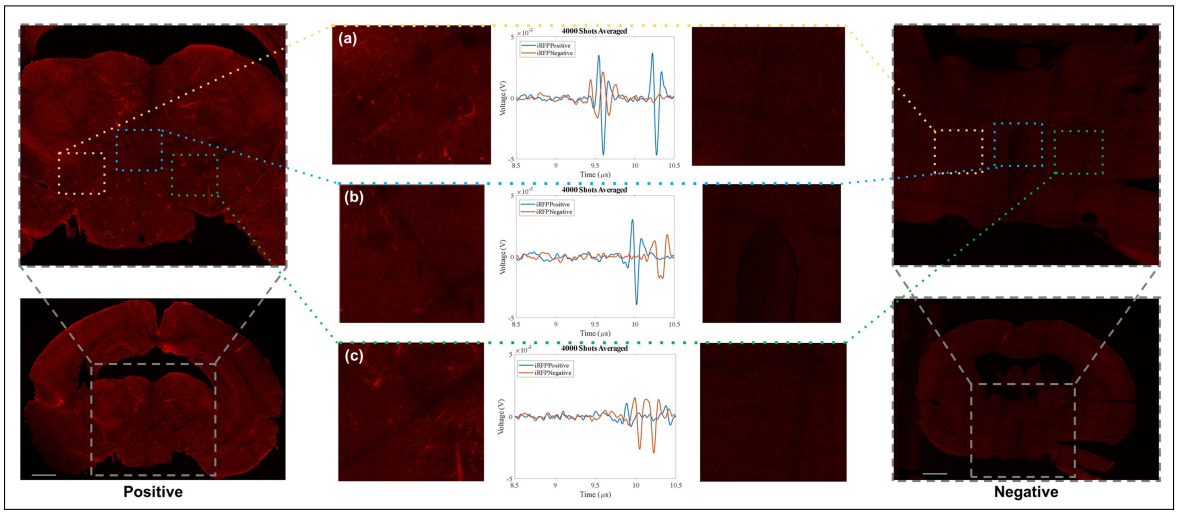

Figure 4.4: Confocal Images of IRFP Expression in Fixed Coronal Brain Sections of DAT:Cre Positive and Wild-type Negative Mice Injected with AAV1-EF1a-DIO-Nuc-IRFP. Scale Bar Is 1 mm. DAT:Cre Positive Mice Show Extensive IRFP Expression Throughout the Brain. Highlighted Blue, Green, and Yellow Boxes Show the Approximate Area That Brain Slices Were Scanned by Photoacoustic Microscopy. Corresponding Data Shows the Photoacoustic Signal from IRFP Positive and IRFP Negative Brains Slices, Indicating a Higher Photoacoustic Signal in the IRFP Positive Areas Scanned.

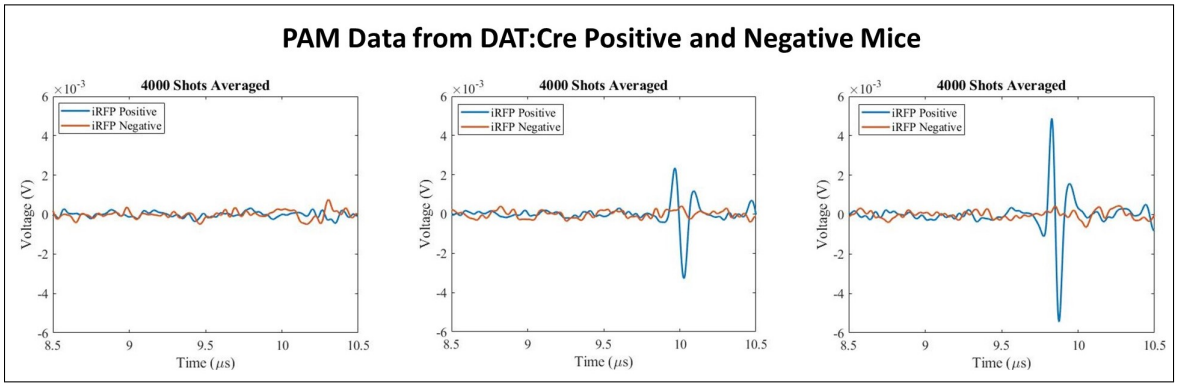

Figure 4.5: Additional PAM Data Shows the Photoacoustic Signal from IRFP Positive And IRFP Negative Brains Slices, Indicating a Higher Photoacoustic Signal in the IRFP Positive Areas Scanned.

cells for targeting in combination with an overhead LED light to stimulate fluorescence for further cell targeting. Though the system is currently capable of brightfield imaging, these additions would allow dual PA and fluorescence imaging of both brain slices and cells in culture within the same system. One further limitation of our study is the inconsistent expression of iRFP in brain slices. Though we did see the expression of iRFP in cells that correlated with Cre and TH expression in the mouse midbrain in DAT:Cre positive mice, we also saw expression outside of areas with TH. Future studies will have AAV injections targeted to the midbrain region, and temporal expression of Cre will be controlled using conditional mice. Using these genetic targeting strategies with more advanced PA imaging technologies such as acoustic resolution PAM and PAT will also greatly increase the depth of detection of these proteins.

4.3.4 Conclusion

In summary, we have developed and optimized a PAM system to evaluate iRFP in neuronal cells in brain slices. This system was able to detect iRFP expression in brain sections of transgenic mice that were transfected using AAV vectors. This study is a first step toward developing PA technologies that work in concert with the expression of reporter proteins through Cre recombination. Though we did not investigate the depth of detection for these genetically encoded contrast agents, we believe that combining these strategies alongside advanced PA imaging technologies could greatly expand the capabilities of neuroscientists in studies of the brain. This

study is a first step towards expanding the cell types and processes that neuroscience can image beyond the optical diffusion limit.

Chapter 5

CONCLUSIONS AND FUTURE WORK

This chapter outlines the major significance and contributions of each of the specific aims that were described in the dissertation. In addition, it provides insight into the publications and conference presentations that contributed to the production of this dissertation. Finally, it provides directions for future work that could expand upon the research presented.

5.1 Significance and Contributions

5.1.1 Chapter 2

Ovarian cancer is the deadliest gynecological cancer and is often detected at a late stage.[118,122] To address the critical need for new technologies for ovarian cancer detection, we built a novel PAFC system to identify ovarian CTCs in flow utilizing CuS NPs. We described the synthesis of CuS NPs with folic acid as a capping agent and characterized them by TEM, DLS, and MALDI-TOFMS. This characterization demonstrated that we successfully conjugated our nanoparticles to folic acid and their suitability for use in PA experiments, making them an ideal contrast agent for the PA detection of ovarian CTCs. We then successfully conjugated these nanoparticles to fluorescent compounds and visualized their uptake into SKOV-3 ovarian cancer cells.

These studies are the first to demonstrate the ability of CuS NPs to be utilized as contrast agents for the PA detection of ovarian CTCs in flow. To detect these ovarian CTCs, a custom PAFC system was developed. The PAFC system was designed in Solidworks and 3D printed to allow for the passage of cells through a central capillary. These cells were then illuminated by a fiber optic cable adjacent to an ultrasound transducer to detect PA signal. We then tested cells after they were incubated with FA-CuS NPs. We identified significantly higher PA signals in the NP-tagged cells versus cells that were not tagged with NPs and PBS. These studies demonstrate the systems' ability to detect cells down to a concentration of 1 cell/μl.

In this aim, we utilized PAFC to detect ovarian cancer cells in flow using FA-CuS NPs. With this system, we detected ovarian CTCs at physiologically relevant concentrations (1 cell/μl). Outcomes from this work led to the publication of a detailed protocol, including the 3D model for the flow system and a detailed protocol for FA-CuS NP synthesis, enabling other researchers to replicate this approach.[85] Through this work, we tested the utility of CuS NPs to detect ovarian CTCs. The PAFC and NP systems developed in this study provide tools that enable further cellular detection and characterization of analytes using PA.

5.1.2 Chapter 3

Technologies capable of imaging NIR contrast in neuronal cells at increased depth *in vitro* are necessary to expand the capabilities of neuroscientists. To address this need, we built a custom NIR PAM system designed to identify iRFP. This system

applied a 700 nm wavelength to excite iRFP and generate a PA signal. To evaluate this system, we generated a monoclonal iRFP cell line, and isolated cells with high iRFP expression. Through this work, we demonstrated dual PA and fluorescence contrast detection of iRFP in neuroblastoma cells. Ultimately, we demonstrated the successful development of a system capable of detecting the presence of these genetically encoded PA and fluorescence contrast agents. This is the first time, to the author's knowledge, that genetically encoded iRFP has been detected in neuronal cell types utilizing PA.

The significance of the resulting data from these studies has implications for detecting iRFPs in select neuronal cell types and can be further extrapolated to characterize a wide variety of genetically encoded contrast agents. This system can be further utilized to evaluate a variety of NIR PA contrast agents including FRET sensors, calcium indicators, and photoswithcable probes. Overall, we demonstrated the construction of a custom NIR-PAM system that can detect iRFP in B35 cells. Future studies aim to expand this system to investigate a variety of genetically encoded PA contrast agents.

5.1.3 Chapter 4

Neuroscientists have been limited to the cortical surface when imaging neuronal subtypes in the brain using traditional microscopy methods. To address the need for an increased depth of imaging, we applied our custom PAM system (**Chapter 3**) to detect iRFP in brain slices. The expression of iRFP was accomplished by injecting

an AAV, specifically designed to produce iRFP in a Cre-dependent manner, into neonatal DAT:Cre mice. After an incubation period, the mice were intracardially perfused and their brains were removed and cryopreserved. The brains were then sectioned by a cryostat and evaluated for iRFP expression through IHC and PA. IHC showed iRFP expression that correlated with Cre recombinase and colocalized with tyrosine hydroxylase, suggesting positive iRFP expression in mice in a Cre-dependent manner. In addition, DAT:Cre positive brain sections were scanned and compared with DAT:Cre negative sections that were also injected with AAV. Results indicate significantly increased PA signal in the brain sections expressing iRFP. Our data suggests successful detection of iRFP in brain sections expressing iRFP in a Cre-dependent manner.

Several studies have explored the PA effect of iRFP in cells, however, no studies to date have utilized PAM to detect neuronal cells in brain slices. Furthermore, to the best of our knowledge, no studies have utilized the Cre/Recombinase system to express PA contrast agents. The combination of Cre/lox recombination with PA addresses a critical need to adapt the genetic tools developed by neuroscientists to study the brain using PA. Through this work, we produced PA contrast agents in transgenic mice and detected signals via our custom-built PAM system. The demonstration of this detection strategy is significant as it expands the potential use of PA within neuroscience applications.

5.1.4 Contributions

The following is a list of peer-reviewed publications and conference oral and poster presentations that contributed to this dissertation.

List of Publications

- Miranda, C., Howell, M. R., **Lusk, J. F.**, Marschall, E., Eshima, J., Anderson, T., Smith, B. S. "Automated microscope-independent fluorescence guided micropipette." *Biomedical Optics Express* 12(8), 4689-4699.

- **Lusk, Joel**, et al. "Photoacoustic Flow System for the Detection of Ovarian Circulating Tumor Cells Utilizing Copper Sulfide Nanoparticles." *ACS Biomaterials Science and Engineering* 5(3) (2019): 1553-1560.

- **Lusk, Joel**, et al. "Ovarian Cancer Detection Using Photoacoustic Flow Cytometry." *JOVE* 19 (2020): 100167.

- Johnston, S. A., Domenyuk, V., Gupta, N., Batista, M. T., Lainson, J. C., Zhao, Z. G., **Lusk, J.F.**, et al. "A Simple Platform for the Rapid Development of Antimicrobials. " *Scientific Reports* 7(1) (2017): 1-11

List of Poster Presentations

- **Joel Lusk**, Christopher Miranda, and Barbara Smith. "Treatment and Diagnosis of Cervical Cancer Using Photoacoustic Nanoparticle Contrast Agents Synthesized by Green Methods" **Molecular, Cellular and Tissue Bioengineering Symposium**, Tempe, AZ March, 2017

- Madeleine Howell, **Joel Lusk**, Christopher Miranda, and Barbara Smith. "Aggregation of copper sulfide nanoparticles around nanoscale targets for photoacoustic contrast in a flow model" **Biomedical Engineering Society Annual Meeting** Tempe, AZ, March 2017

- **Joel Lusk**, Christopher Miranda, and Barbara Smith. "Nanoparticle Contrast Agents for use in Photoacoustic Imaging for the Early Detection and Photothermal Ablation of Ovarian Cancer" **Molecular, Cellular and Tissue Bioengineering Symposium** Tempe, AZ, March 2017

- **Joel Lusk**, Christopher Miranda, Matthew Chrest, and Barbara Smith. ""Copper Sulfide Nanoparticles for the Detection of Circulating Ovarian Cancer Cells in a Photoacoustic Flow System" **Molecular, Cellular and Tissue Bioengineering Symposium** Tempe, AZ, March 2018

- Christopher Miranda, Madeleine Howell, **Joel Lusk**, Ethan Marschall, Barbara S. Smith. "Photoacoustic and Fluorescence Guided Electrophysiology"" **Biomedical Engineering Society Annual Meeting** Philadelphia, PA. October 2019

- Christopher Miranda, Madeleine Howell, **Joel Lusk**, Ethan Marschall, Barbara S. Smith. "Fluorescence-Guided Electrophysiology." **Biomedical Engineering Society Annual Meeting** Philadelphia, PA. October 2019

- Jarrett Eshima, Esther Sim, **Joel F. Lusk**, Ethan B. Marshall, Barbara S.

Smith "Targeted Photoacoustic Flow System for the Detection of Circulating Ovarian Tumor Cells." **Biomedical Engineering Society Annual Meeting** Philadelphia, PA. October 2019

List of Oral Presentations

- **Joel F. Lusk**, Christopher Miranda, Madeleine Howell, Matthew Chrest, and Barbara S. Smith. "Targeted Photoacoustic Flow System for the Detection of Circulating Ovarian Tumor Cells." **Biomedical Engineering Society Annual Meeting** Atlanta, GA. October 2018

- **Joel F. Lusk**, Christopher Miranda, Ethan Marschall, and Barbara S. Smith. "Photoacoustic Microscopy System for Cell Type Specific Detection Utilizing iRFP." **Biomedical Engineering Society Annual Meeting** Philadelphia, PA October 2019

Provisional Patents

- Provisional U.S. Patent Application **No. 16/798,038** "Folic Acid Functionalized Copper Sulfide Nanoparticles for the Detection of Ovarian Cancer Cells in Flow"

- Provisional U.S. Patent Application **No. 17/321,722** "Photoacoustic Ion Indicators"

- Provisional U.S. Patent **No. 63/171,662** "Devices and Systems for Non-Destructive Collection and Monitoring of Biological Volatiles"

5.2 Project Challenges

We overcame many challenges throughout the pursuit of these aims. In Chapter 2, we explored many different nanoparticle modalities for PA detection. Initially, we synthesized silver glutathione nanoparticles, which generate PA signal and can be used for cell detection. Glutathione was chosen as a capping agent because it is preferentially taken up into cancerous cells due to its antioxidant properties. In preliminary studies, we successfully synthesized silver glutathione nanoparticles and visualized the colocalization of these nanoparticles in HeLa cells (Fig. 5.1). A simple PA experiment was performed, demonstrating that these silver nanoparticles could generate the PA effect (Fig. 5.2). Although we determined that these particles could be taken up into cells and produce the PA effect, there were several disadvantages to utilizing these NPs for our study. First, the silver glutathione nanoparticles had a peak absorbance at a wavelength of approximately 370 nm. Though these silver nanoparticles were suitable for detecting analytes using PA, their low wavelength limited their application in more complex biological systems. In addition, glutathione, which is taken up by many cancer cells, is not sufficiently specific to ovarian cancer cell types. Though these nanoparticles can be further conjugated to various targeting ligands, we sought to utilize a small targeting molecule with higher specificity for ovarian cancer.

We further investigated contrast agents with NIR absorbance in combination with capping ligands that target ovarian cancer cells. After extensive research, it was de-

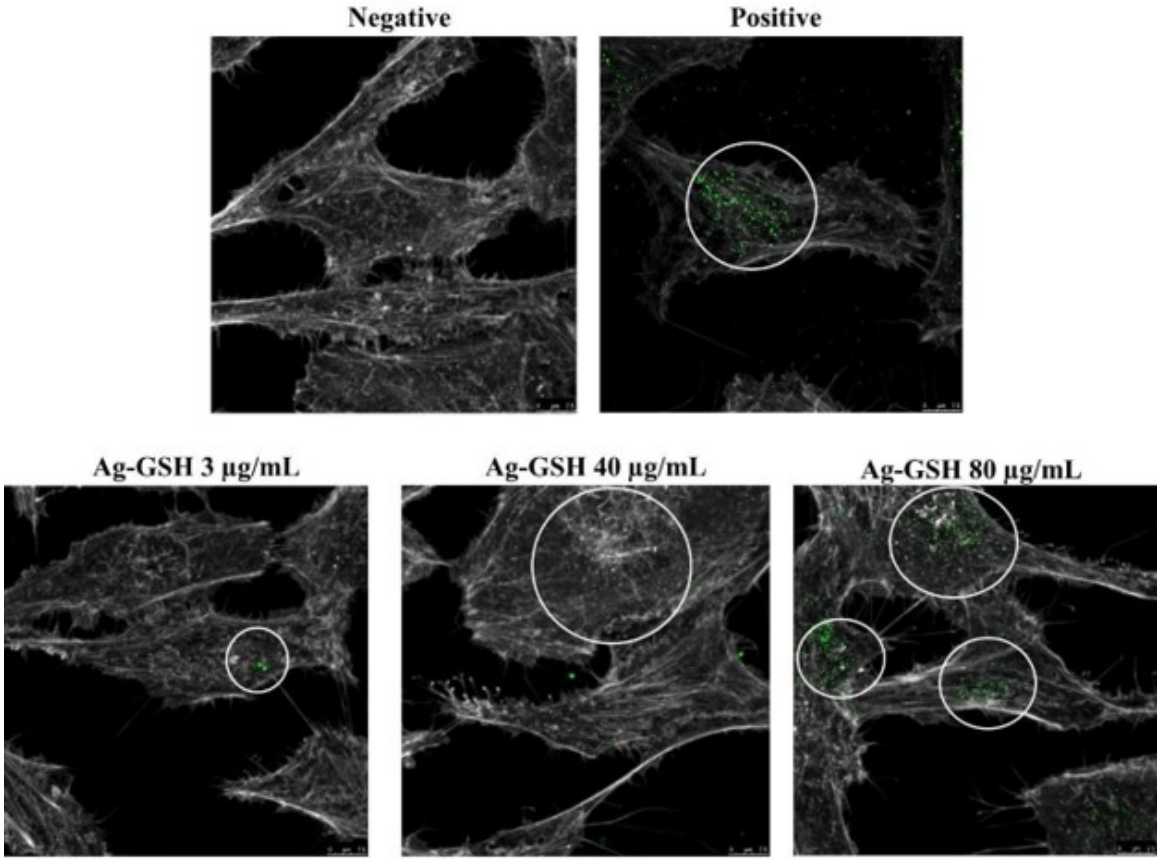

Figure 5.1: Varying Concentrations of Synthesized Day 5 Nanoparticles Were Applied to Cell Culture and Incubated for 24 Hours. The Cells Were Then Imaged by Confocal. Nanoparticles Within Cells Were Imaged Using Reflection Microscopy and Appear Green. White Circles Denote Areas with Nanoparticles. Cells Were Also Stained with Alexafluor-568 Phalloidin (White).

termined that CuS NPs tagged with folic acid were ideal candidates for a nanoparticle system due to their superior absorption in the NIR, and the specificity of folic acid for ovarian cancer cells.[60,86] However, the NP synthesis process lacks considerable information in published protocols. After many attempts to synthesize CuS NPs with ideal properties, we finally produced nanoparticles suitable for our experiments. Due to the lack of available information on CuS NP synthesis, we published a detailed protocol so that other researchers could replicate our method. Another significant

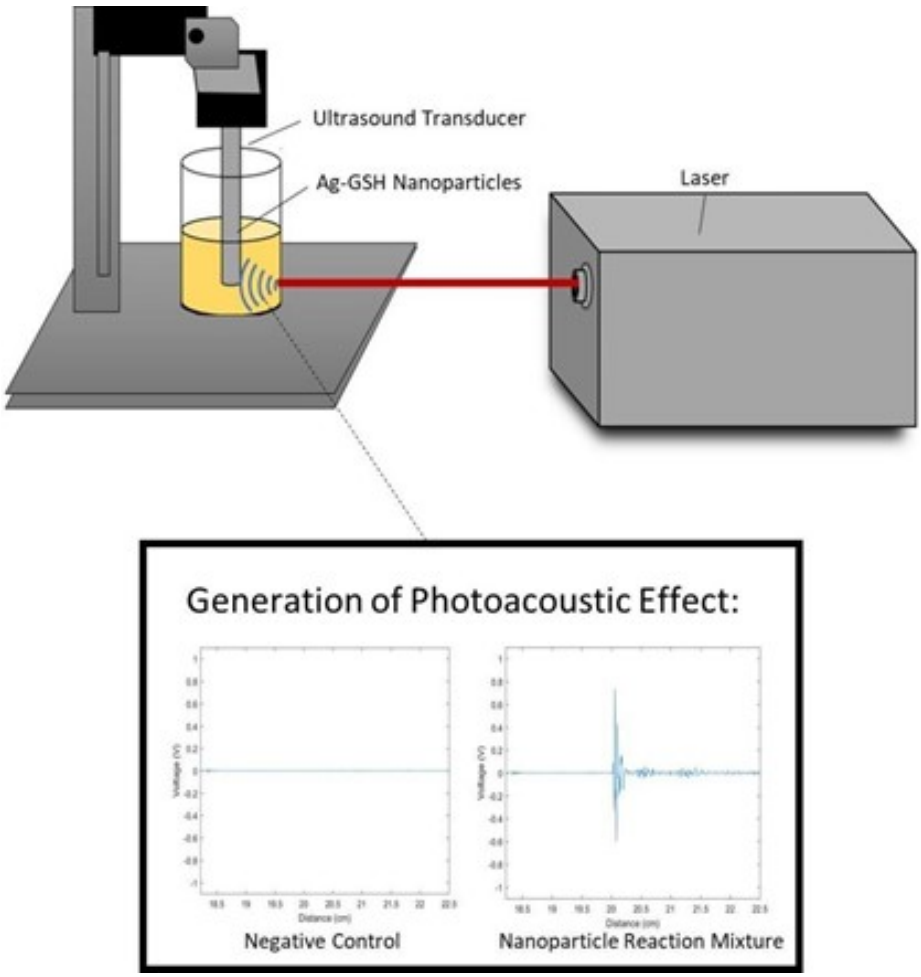

Figure 5.2: Photoacoustic Signal Generation of the Silver Nanoparticle Reaction Mixtures Were Tested by Firing a Laser at a Vial Containing the Nanoparticles and an Ultrasound Transducer. Initial Testing of the Reaction Mixtures Showed the Generation of a Photoacoustic Signal at 432 nm

challenge was the construction of the PAFC system. We worked through many different prototypes before eventually creating the flow system in its current iteration that could reliably detect analytes utilizing PA. Once again, we published a detailed protocol on its construction that included 3D printed files for the flow system so that these systems could more easily be replicated. In addition to publishing protocols describing these technologies, we have also filed a provisional patent for these tech-

nologies and presented our research at the Biomedical Engineering Society conference in Atlanta, GA.

For Chapter 3, we faced considerable challenges while constructing the PAM system and analyzing cells *in vitro*. Though data from an early version of the PAM system shows the ability to image carbon fibers that were 254 and 7.2 µm (Fig. 5.3 and 5.4), due to limitations in the firing rate of the laser, and the lower extinction coefficient of iRFP than carbon, scanning cells took significantly longer than the carbon fibers. In addition to long scanning times, we also had fluctuations in the laser power over extended periods. These fluctuations were significant enough across long scans (several hours) to augment the resulting PA data. We initially attempted to image individual cells in the PAM system, however, after extensive scanning and careful calibration no signal was identified. The inability to scan single cells led us to eventually examine cells in agarose gels. We successfully scanned these agarose gels and were reliably able to produce a PA signal from iRFP transfected cells as compared to the negative controls. The resulting data gathered from these agarose gels gave us further confidence to use our system to detect iRFP in brain slices.

In Chapter 4, we encountered additional challenges. Initial experiments were performed on Nex:Cre mice due to their extensive expression of Cre throughout the cortex, making them a good model for the positive expression of Cre-dependent reporter proteins. However, after preliminary experiments, where AAV1-DIO-Nuc-IRFP was injected into the cortex, our results failed to show expression of iRFP.

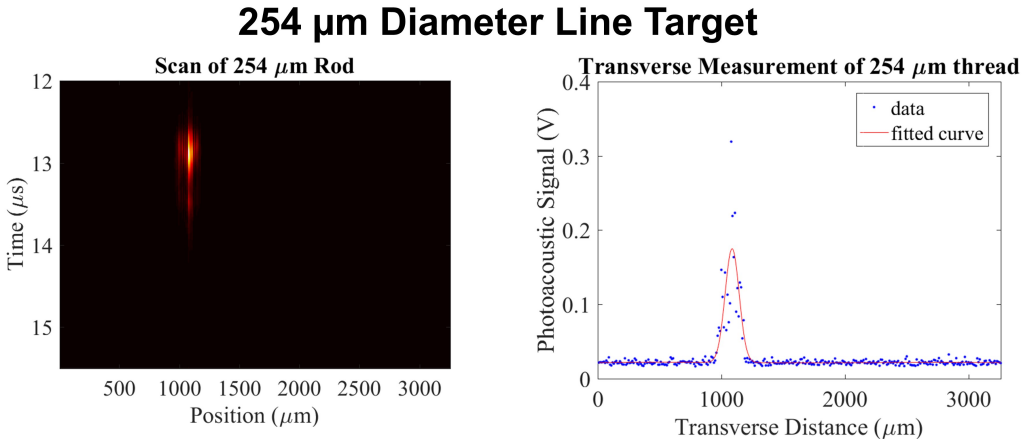

Figure 5.3: (A) Preliminary PAM Data Shows the Photoacoustic Reconstruction and Transverse Measurement of a 254-µm Carbon Fiber.

We then changed our mouse model to DAT:Cre to study dopaminergic cells in the midbrain. We transitioned to the ICV injection of neonatal mice as it equally distributes the AAV throughout the brain. In addition, this method is much easier to perform than intracranial injections through a craniotomy. Ultimately, we successfully expressed iRFP in brain slices and characterized these brain slices by PAM. Some sporadic iRFP expression was present in mice injected with AAVs. Further experiments will seek to restrict iRFP expression through targeted injections and tamoxifen induced Cre expression. Overall, we overcame these challenges to eventually express iRFPs in DAT:Cre mice.

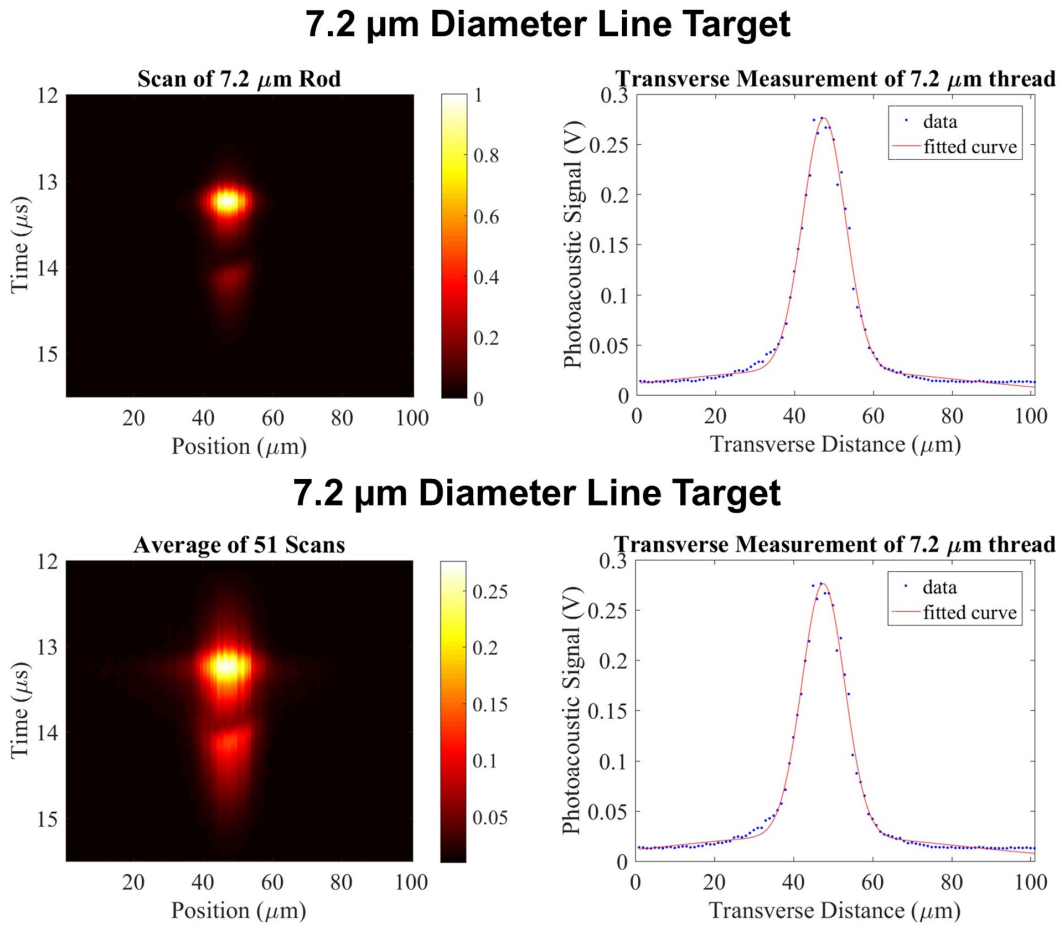

Figure 5.4: (Top) Photoacoustic Reconstruction and Transverse Measurement of Single Line Scan of a 7.2- µm Carbon Fiber. (Bottom) Photoacoustic Reconstruction and Transverse Measurement of an Average of 51 Line Scans of a 7.2- µm Carbon Fiber.

5.3 Future Work

Ultimately, in Chapter 2, we were able to demonstrate the ability of this system to detect isolated ovarian CTCs *in vitro*. The ability to identify particular CTCs amongst a variety of cell types is important as an initial step to show the systems' utility to identify cells in a clinical setting. Further studies will consider cells in co-culture to confirm the selective identification of ovarian CTCs. Future studies

can also apply this system to clinical samples and *in vivo* models. One of the main advantages of this PA system over traditional fluorescence microscopy is its ability to penetrate more deeply into tissues. For clinical translation, blood analysis should first be performed using ex vivo blood and serum samples. Through this work, our overarching goal is to ultimately distinguish cells in complex biological systems such as blood. This can be accomplished by utilizing these FA-CuS NPs in combination with PAFC.

PAFC has been used in multiple applications to detect cells *in vivo*, including melanomas and gold nanoparticle-tagged cancer cells.[96,164] Due to recent studies that suggest the biocompatibility of these nanoparticles, these contrast agents and a modified version of this system could potentially be utilized to study nanoparticles within *in vivo* models.[115] Though few new nanoparticles are approved for human use, these tools show promise for clinical and research translation. In addition, the folic acid that is present on the surface of these NPs provides an easy site for conjugation to a variety of additional targeting moieties, such as antibodies. This is demonstrated in Chapter 2 where we tagged the nanoparticles with a fluorescent compound. The fluorescence conjugation was performed by utilizing a NHS-Texas red dye. The ability to direct these nanoparticles to a wide variety of targets by conjugating them to additional targeting ligands makes this system useful for a variety of applications.

For Chapter 3, additional studies can utilize the custom PAM system to further characterize cell types and molecular PA contrast agents *in vitro*. The iRFP proteins

utilized in this research have been adapted for a variety of purposes. Monomeric versions of these proteins used for protein interaction imaging and photoswitchable iRFPs have also been developed that increase the ability to view these proteins utilizing PA.[149,67] In addition, several new NIR calcium indicators have been developed that can visualize the firing of neuronal cells.[104] More recently, NIR voltage indicators have emerged that allow for the more direct imaging of action potentials in cells.[114] This PAM system, due to its ability to characterize the expression of NIR proteins *in vitro*, could also be used to characterize a variety of these additional NIR fluorescent proteins in primary and immortalized cell lines.

Furthermore, by implementing different lasers, our current PAM system could easily be updated to an OR-PAM system to enable individual cellular imaging at optical resolution. Our PAM system has been outfitted with a camera to be easily converted to a fluorescence microscopy system. With the addition of a fluorescence light source and fluorescent filters in the beam path, the system could accommodate simultaneous fluorescent and PA microscopy. Future studies will examine the incorporation of this system into a traditional fluorescence microscope. The ability to easily use the optics of a traditional microscopy platform to house this PAM system would significantly enhance the ability of other researchers to utilize this platform.

In Chapter 4 of the dissertation, we demonstrate the ability to detect PA signals from iRFP in transgenically modified mice. To the best of the author's knowledge, this demonstrates the first time a study has looked at neuronal cells characterized by

PA in brain slices. This work has far-reaching implications for future neuroscience studies. Though this study only characterized iRFP in fixed tissues, in the future, the system could be used to characterize these proteins in live brain sections. This work also has further implications for the characterization of iRFP in a variety of cell types for targeting electrophysiology. Finally, this system could ultimately be utilized to visualize a wide range of genetically encoded NIR proteins in studies of neuronal subtypes *in vivo*.

REFERENCES

[1] Adachi, T. and Y. Nakamura, "Aptamers: A review of their chemical properties and modifications for therapeutic application", Molecules **24**, 23, 4229 (2019).

[2] Allard, W. J., J. Matera, M. C. Miller, M. Repollet, M. C. Connelly, C. Rao, A. G. Tibbe, J. W. Uhr and L. W. Terstappen, "Tumor cells circulate in the peripheral blood of all major carcinomas but not in healthy subjects or patients with nonmalignant diseases", Clinical cancer research **10**, 20, 6897–6904 (2004).

[3] Armstrong, D. K., "Relapsed ovarian cancer: challenges and management strategies for a chronic disease", The oncologist **7**, 20–28 (2002).

[4] Assaraf, Y. G., C. P. Leamon and J. A. Reddy, "The folate receptor as a rational therapeutic target for personalized cancer treatment", Drug Resistance Updates **17**, 4-6, 89–95 (2014).

[5] Benninger, R. K. and D. W. Piston, "Two-photon excitation microscopy for the study of living cells and tissues", Current protocols in cell biology **59**, 1, 4–11 (2013).

[6] Bhagwat, N., K. Dulmage, C. H. Pletcher, L. Wang, W. DeMuth, M. Sen, D. Balli, S. S. Yee, S. Sa, F. Tong *et al.*, "An integrated flow cytometry-based platform for isolation and molecular characterization of circulating tumor single cells and clusters", Scientific reports **8**, 1, 1–14 (2018).

[7] Bhattacharyya, K., B. S. Goldschmidt and J. A. Viator, "Detection and capture of breast cancer cells with photoacoustic flow cytometry", Journal of biomedical optics **21**, 8, 087007 (2016).

[8] Blassl, C., J. D. Kuhlmann, A. Webers, P. Wimberger, T. Fehm and H. Neubauer, "Gene expression profiling of single circulating tumor cells in ovarian cancer–establishment of a multi-marker gene panel", Molecular oncology **10**, 7, 1030–1042 (2016).

[9] Bocarsly, M. E., W.-c. Jiang, C. Wang, J. T. Dudman, N. Ji and Y. Aponte, "Minimally invasive microendoscopy system for in vivo functional imaging of deep nuclei in the mouse brain", Biomedical Optics Express **6**, 11, 4546–4556 (2015).

[10] Bodea, S.-V. and G. G. Westmeyer, "Photoacoustic neuroimaging-perspectives on a maturing imaging technique and its applications in neuroscience", Frontiers in Neuroscience **15** (2021).

[11] Brand, C., A. Sadique, J. L. Houghton, K. Gangangari, J. F. Ponte, J. S. Lewis, N. V. K. Pillarsetty, J. A. Konner and T. Reiner, "Leveraging pet to image folate receptor α therapy of an antibody-drug conjugate", EJNMMI research **8**, 1, 1–10 (2018).

[12] Brunker, J., J. Yao, J. Laufer and S. E. Bohndiek, "Photoacoustic imaging using genetically encoded reporters: a review", Journal of biomedical optics **22**, 7, 070901 (2017).

[13] Cai, C., D. A. Nedosekin, Y. A. Menyaev, M. Sarimollaoglu, M. A. Proskurnin and V. P. Zharov, "Photoacoustic flow cytometry for single sickle cell detection in vitro and in vivo", Analytical Cellular Pathology **2016** (2016).

[14] Campbell, R. E., O. Tour, A. E. Palmer, P. A. Steinbach, G. S. Baird, D. A. Zacharias and R. Y. Tsien, "A monomeric red fluorescent protein", Proceedings of the National Academy of Sciences **99**, 12, 7877–7882 (2002).

[15] Cao, Y., A. Kole, J. Hui, Y. Zhang, J. Mai, M. Alloosh, M. Sturek and J.-X. Cheng, "Fast assessment of lipid content in arteries in vivo by intravascular photoacoustic tomography", Scientific reports **8**, 1, 1–10 (2018).

[16] Capozza, M., F. Blasi, G. Valbusa, P. Oliva, C. Cabella, F. Buonsanti, A. Cordaro, L. Pizzuto, A. Maiocchi and L. Poggi, "Photoacoustic imaging of integrin-overexpressing tumors using a novel icg-based contrast agent in mice", Photoacoustics **11**, 36–45 (2018).

[17] Chalfie, M., Y. Tu, G. Euskirchen, W. W. Ward and D. C. Prasher, "Green fluorescent protein as a marker for gene expression", Science **263**, 5148, 802–805 (1994).

[18] Chen, J., V. P. Nguyen, S. Jaiswal, X. Kang, M. Lee, Y. M. Paulus and T. D. Wang, "Thin layer-protected gold nanoparticles for targeted multimodal imaging with photoacoustic and ct", Pharmaceuticals **14**, 11, 1075 (2021).

[19] Chien, Y.-F., J.-Y. Lin, P.-T. Yeh, K.-J. Hsu, Y.-H. Tsai, S.-K. Chen and S.-W. Chu, "Dual grin lens two-photon endoscopy for high-speed volumetric and deep brain imaging", Biomedical Optics Express **12**, 1, 162–172 (2021).

[20] D Friedman, A., S. E Claypool and R. Liu, "The smart targeting of nanoparticles", Current pharmaceutical design **19**, 35, 6315–6329 (2013).

[21] Daskalaki, A., S. Agelaki, M. Perraki, S. Apostolaki, N. Xenidis, E. Stathopoulos, E. Kontopodis, D. Hatzidaki, D. Mavroudis and V. Georgoulias, "Detection of cytokeratin-19 mrna-positive cells in the peripheral blood and bone marrow of patients with operable breast cancer", British journal of cancer **101**, 4, 589–597 (2009).

[22] de Albuquerque, A., S. Kaul, G. Breier, P. Krabisch and N. Fersis, "Multimarker analysis of circulating tumor cells in peripheral blood of metastatic breast cancer patients: a step forward in personalized medicine", Breast Care **7**, 1, 7–12 (2012).

[23] de la Zerda, A., S. Bodapati, R. Teed, S. Y. May, S. M. Tabakman, Z. Liu, B. T. Khuri-Yakub, X. Chen, H. Dai and S. S. Gambhir, "Family of enhanced photoacoustic imaging agents for high-sensitivity and multiplexing studies in living mice", ACS nano **6**, 6, 4694–4701 (2012).

[24] Deliolanis, N. C., A. Ale, S. Morscher, N. C. Burton, K. Schaefer, K. Radrich, D. Razansky and V. Ntziachristos, "Deep-tissue reporter-gene imaging with fluorescence and optoacoustic tomography: a performance overview", Molecular imaging and biology **16**, 5, 652–660 (2014).

[25] Duncan, R. and R. Gaspar, "Nanomedicine (s) under the microscope", Molecular pharmaceutics **8**, 6, 2101–2141 (2011).

[26] Fan, T., Q. Zhao, J. J. Chen, W.-T. Chen and M. L. Pearl, "Clinical significance of circulating tumor cells detected by an invasion assay in peripheral blood of patients with ovarian cancer", Gynecologic oncology **112**, 1, 185–191 (2009).

[27] Ferlay, J., M. Colombet, I. Soerjomataram, C. Mathers, D. Parkin, M. Piñeros, A. Znaor and F. Bray, "Estimating the global cancer incidence and mortality in 2018: Globocan sources and methods", International journal of cancer **144**, 8, 1941–1953 (2019).

[28] Filippi, M., F. Garello, C. Pasquino, F. Arena, P. Giustetto, F. Antico and E. Terreno, "Indocyanine green labeling for optical and photoacoustic imaging of mesenchymal stem cells after in vivo transplantation", Journal of Biophotonics **12**, 5, e201800035 (2019).

[29] Filonov, G. S., A. Krumholz, J. Xia, J. Yao, L. V. Wang and V. V. Verkhusha, "Deep-tissue photoacoustic tomography of a genetically encoded near-infrared fluorescent probe", Angewandte Chemie **124**, 6, 1477–1480 (2012).

[30] Filonov, G. S., K. D. Piatkevich, L.-M. Ting, J. Zhang, K. Kim and V. V. Verkhusha, "Bright and stable near-infrared fluorescent protein for in vivo imaging", Nature biotechnology **29**, 8, 757–761 (2011).

[31] Fu, Q., R. Zhu, J. Song, H. Yang and X. Chen, "Photoacoustic imaging: contrast agents and their biomedical applications", Advanced Materials **31**, 6, 1805875 (2019).

[32] Galanzha, E. I., Y. A. Menyaev, A. C. Yadem, M. Sarimollaoglu, M. A. Juratli, D. A. Nedosekin, S. R. Foster, A. Jamshidi-Parsian, E. R. Siegel, I. Makhoul

et al., "In vivo liquid biopsy using cytophone platform for photoacoustic detection of circulating tumor cells in patients with melanoma", Science translational medicine **11**, 496, eaat5857 (2019).

[33] Galanzha, E. I., E. Shashkov, M. Sarimollaoglu, K. E. Beenken, A. G. Basnakian, M. E. Shirtliff, J.-W. Kim, M. S. Smeltzer and V. P. Zharov, "In vivo magnetic enrichment, photoacoustic diagnosis, and photothermal purging of infected blood using multifunctional gold and magnetic nanoparticles", (2012).

[34] Galanzha, E. I., E. V. Shashkov, T. Kelly, J.-W. Kim, L. Yang and V. P. Zharov, "In vivo magnetic enrichment and multiplex photoacoustic detection of circulating tumour cells", Nature nanotechnology **4**, 12, 855–860 (2009).

[35] Galanzha, E. I. and V. P. Zharov, "Photoacoustic flow cytometry", Methods **57**, 3, 280–296 (2012).

[36] Galanzha, E. I. and V. P. Zharov, "Circulating tumor cell detection and capture by photoacoustic flow cytometry in vivo and ex vivo", Cancers **5**, 4, 1691–1738 (2013).

[37] Gao, W., Y. Sun, M. Cai, Y. Zhao, W. Cao, Z. Liu, G. Cui and B. Tang, "Copper sulfide nanoparticles as a photothermal switch for trpv1 signaling to attenuate atherosclerosis", Nature communications **9**, 1, 1–10 (2018).

[38] Gnesin, S., J. Müller, I. A. Burger, A. Meisel, M. Siano, M. Früh, M. Choschzick, C. Müller, R. Schibli, S. M. Ametamey *et al.*, "Radiation dosimetry of 18f-azafol: A first in-human use of a folate receptor pet tracer", EJNMMI research **10**, 1, 1–12 (2020).

[39] Gorges, T. M., I. Tinhofer, M. Drosch, L. Röse, T. M. Zollner, T. Krahn and O. Von Ahsen, "Circulating tumour cells escape from epcam-based detection due to epithelial-to-mesenchymal transition", BMC cancer **12**, 1, 1–13 (2012).

[40] Guo, H., Y. Li, W. Qi and L. Xi, "Photoacoustic endoscopy: A progress review", Journal of Biophotonics **13**, 12, e202000217 (2020).

[41] Guo, L., I. Panderi, D. D. Yan, K. Szulak, Y. Li, Y.-T. Chen, H. Ma, D. B. Niesen, N. Seeram, A. Ahmed *et al.*, "A comparative study of hollow copper sulfide nanoparticles and hollow gold nanospheres on degradability and toxicity", ACS nano **7**, 10, 8780–8793 (2013).

[42] Hannah, A., G. Luke, K. Wilson, K. Homan and S. Emelianov, "Indocyanine green-loaded photoacoustic nanodroplets: dual contrast nanoconstructs for enhanced photoacoustic and ultrasound imaging", ACS nano **8**, 1, 250–259 (2014).

[43] Hawes, R. H., Q. Xiong, I. Waxman, K. J. Chang, D. B. Evans and J. L. Abbruzzese, "A multispecialty approach to the diagnosis and management of pancreatic cancer", The American journal of gastroenterology **95**, 1, 17–31 (2000).

[44] He, W., S. A. Kularatne, K. R. Kalli, F. G. Prendergast, R. J. Amato, G. G. Klee, L. C. Hartmann and P. S. Low, "Quantitation of circulating tumor cells in blood samples from ovarian and prostate cancer patients using tumor-specific fluorescent ligands", International journal of cancer **123**, 8, 1968–1973 (2008).

[45] Heim, R. and R. Y. Tsien, "Engineering green fluorescent protein for improved brightness, longer wavelengths and fluorescence resonance energy transfer", Current biology **6**, 2, 178–182 (1996).

[46] Icon, A. Collaborators *et al.*, "Paclitaxel plus platinum-based chemotherapy versus conventional platinum-based chemotherapy in women with relapsed ovarian cancer: the icon4/ago-ovar-2.2 trial", The Lancet **361**, 9375, 2099–2106 (2003).

[47] Imai, T., B. Muz, C.-H. Yeh, J. Yao, R. Zhang, A. K. Azab and L. Wang, "Direct measurement of hypoxia in a xenograft multiple myeloma model by optical-resolution photoacoustic microscopy", Cancer biology & therapy **18**, 2, 101–105 (2017).

[48] Jacobs, I. J. and U. Menon, "Progress and challenges in screening for early detection of ovarian cancer", Molecular & Cellular Proteomics **3**, 4, 355–366 (2004).

[49] Jelovac, D. and D. K. Armstrong, "Recent progress in the diagnosis and treatment of ovarian cancer", CA: a cancer journal for clinicians **61**, 3, 183–203 (2011).

[50] Jeon, S., J. Kim, D. Lee, J. W. Baik and C. Kim, "Review on practical photoacoustic microscopy", Photoacoustics **15**, 100141 (2019).

[51] Jiang, J., H. Zhao, W. Shu, J. Tian, Y. Huang, Y. Song, R. Wang, E. Li, D. Slamon, D. Hou *et al.*, "An integrated microfluidic device for rapid and high-sensitivity analysis of circulating tumor cells", Scientific reports **7**, 1, 1–11 (2017).

[52] Jung, H., S. Park, G. R. Gunassekaran, M. Jeon, Y.-E. Cho, M.-C. Baek, J. Y. Park, G. Shim, Y.-K. Oh, I.-S. Kim *et al.*, "A peptide probe enables photoacoustic-guided imaging and drug delivery to lung tumors in k-rasla2 mutant mice", Cancer research **79**, 16, 4271–4282 (2019).

[53] Khoury-Collado, F. and D. S. Chi, "Recent surgical management of ovarian cancer", Journal of Obstetrics and Gynaecology Research **37**, 5, 379–382 (2011).

[54] Kim, G., S.-W. Huang, K. C. Day, M. O'Donnell, R. R. Agayan, M. A. Day, R. Kopelman and S. Ashkenazi, "Indocyanine-green-embedded pebbles as a contrast agent for photoacoustic imaging", Journal of biomedical optics **12**, 4, 044020 (2007).

[55] Kim, J.-W., E. I. Galanzha, E. V. Shashkov, H.-M. Moon and V. P. Zharov, "Golden carbon nanotubes as multimodal photoacoustic and photothermal high-contrast molecular agents", Nature nanotechnology **4**, 10, 688–694 (2009).

[56] Kim, J.-Y., S. D. Grunke, Y. Levites, T. E. Golde and J. L. Jankowsky, "Intracerebroventricular viral injection of the neonatal mouse brain for persistent and widespread neuronal transduction", JoVE (Journal of Visualized Experiments) , 91, e51863 (2014).

[57] Kim, S.-E., B.-R. Lee, H. Lee, S. D. Jo, H. Kim, Y.-Y. Won and J. Lee, "Near-infrared plasmonic assemblies of gold nanoparticles with multimodal function for targeted cancer theragnosis", Scientific reports **7**, 1, 1–10 (2017).

[58] Kipps, E., D. S. Tan and S. B. Kaye, "Meeting the challenge of ascites in ovarian cancer: new avenues for therapy and research", Nature Reviews Cancer **13**, 4, 273–282 (2013).

[59] Krumholz, A., D. M. Shcherbakova, J. Xia, L. V. Wang and V. V. Verkhusha, "Multicontrast photoacoustic in vivo imaging using near-infrared fluorescent proteins", Scientific reports **4**, 1, 1–7 (2014).

[60] Ku, G., M. Zhou, S. Song, Q. Huang, J. Hazle and C. Li, "Copper sulfide nanoparticles as a new class of photoacoustic contrast agent for deep tissue imaging at 1064 nm", ACS nano **6**, 8, 7489–7496 (2012).

[61] Kuipers, E. and J. Haringsma, "Diagnostic and therapeutic endoscopy", Journal of Surgical Oncology **92**, 3, 203–209 (2005).

[62] Kuriu, Y., E. Otsuji, S. Kin, Y. Nakase, K.-I. Fukuda, K. Okamoto, A. Hagiwara and H. Yamagishi, "Monoclonal antibody conjugated to gadolinium as a contrast agent for magnetic resonance imaging of human rectal carcinoma", Journal of surgical oncology **94**, 2, 144–148 (2006).

[63] Lecoq, J., N. Orlova and B. F. Grewe, "Wide. fast. deep: recent advances in multiphoton microscopy of in vivo neuronal activity", Journal of Neuroscience **39**, 46, 9042–9052 (2019).

[64] Lee, M., E. J. Kim, Y. Cho, S. Kim, H. H. Chung, N. H. Park and Y.-S. Song, "Predictive value of circulating tumor cells (ctcs) captured by microfluidic device in patients with epithelial ovarian cancer", Gynecologic oncology **145**, 2, 361–365 (2017).

[65] Li, D., L. Humayun, E. Vienneau, T. Vu and J. Yao, "Seeing through the skin: Photoacoustic tomography of skin vasculature and beyond", JID innovations **1**, 3, 100039 (2021).

[66] Li, L., H.-C. Hsu, V. V. Verkhusha, L. V. Wang and D. M. Shcherbakova, "Multiscale photoacoustic tomography of a genetically encoded near-infrared fret biosensor", Advanced Science **8**, 21, 2102474 (2021).

[67] Li, L., A. A. Shemetov, M. Baloban, P. Hu, L. Zhu, D. M. Shcherbakova, R. Zhang, J. Shi, J. Yao, L. V. Wang *et al.*, "Small near-infrared photochromic protein for photoacoustic multi-contrast imaging and detection of protein interactions in vivo", Nature communications **9**, 1, 1–14 (2018).

[68] Li, L. and L. V. Wang, "Recent advances in photoacoustic tomography", BME Frontiers **2021** (2021).

[69] Li, L., J. Xia, G. Li, A. Garcia-Uribe, Q. Sheng, M. A. Anastasio and L. V. Wang, "Label-free photoacoustic tomography of whole mouse brain structures ex vivo", Neurophotonics **3**, 3, 035001 (2016).

[70] Li, L., R. J. Zemp, G. F. Lungu, G. Stoica and L. V. Wang, "Photoacoustic imaging of lacz gene expression in vivo", Journal of biomedical optics **12**, 2, 020504 (2007).

[71] Li, L., L. Zhu, C. Ma, L. Lin, J. Yao, L. Wang, K. Maslov, R. Zhang, W. Chen, J. Shi *et al.*, "Single-impulse panoramic photoacoustic computed tomography of small-animal whole-body dynamics at high spatiotemporal resolution", Nature biomedical engineering **1**, 5, 1–11 (2017).

[72] Li, M., Y. Tang and J. Yao, "Photoacoustic tomography of blood oxygenation: a mini review", Photoacoustics **10**, 65–73 (2018).

[73] Li, P.-C., C.-R. C. Wang, D.-B. Shieh, C.-W. Wei, C.-K. Liao, C. Poe, S. Jhan, A.-A. Ding and Y.-N. Wu, "In vivo photoacoustic molecular imaging with simultaneous multiple selective targeting using antibody-conjugated gold nanorods", Optics Express **16**, 23, 18605–18615 (2008).

[74] Li, W., P. K. Brown, L. V. Wang and Y. Xia, "Gold nanocages as contrast agents for photoacoustic imaging", Contrast media & molecular imaging **6**, 5, 370–377 (2011).

[75] Li, W. and X. Chen, "Gold nanoparticles for photoacoustic imaging", Nanomedicine **10**, 2, 299–320 (2015).

[76] Lin, L., P. Hu, J. Shi, C. M. Appleton, K. Maslov, L. Li, R. Zhang and L. V. Wang, "Single-breath-hold photoacoustic computed tomography of the breast", Nature communications **9**, 1, 1–9 (2018).

[77] Lin, L., P. Hu, X. Tong, S. Na, R. Cao, X. Yuan, D. C. Garrett, J. Shi, K. Maslov and L. V. Wang, "High-speed three-dimensional photoacoustic computed tomography for preclinical research and clinical translation", Nature communications **12**, 1, 1–10 (2021).

[78] Lin, R., J. Chen, H. Wang, M. Yan, W. Zheng and L. Song, "Longitudinal label-free optical-resolution photoacoustic microscopy of tumor angiogenesis in vivo", Quantitative imaging in medicine and surgery **5**, 1, 23 (2015).

[79] Liu, F., Y. Chen, Y. Li, Y. Guo, Y. Cao, P. Li, Z. Wang, Y. Gong and H. Ran, "Folate-receptor-targeted laser-activable poly (lactide-co-glycolic acid) nanoparticles loaded with paclitaxel/indocyanine green for photoacoustic/ultrasound imaging and chemo/photothermal therapy", International journal of nanomedicine **13**, 5139 (2018).

[80] Liu, W. and J. Yao, "Photoacoustic microscopy: principles and biomedical applications", Biomedical engineering letters **8**, 2, 203–213 (2018).

[81] Lu, H. D., B. K. Wilson, A. Heinmiller, B. Faenza, S. Hejazi and R. K. Prud'homme, "Narrow absorption nir wavelength organic nanoparticles enable multiplexed photoacoustic imaging", ACS Applied Materials & Interfaces **8**, 23, 14379–14388 (2016).

[82] Lu, Y., H. Liang, T. Yu, J. Xie, S. Chen, H. Dong, P. J. Sinko, S. Lian, J. Xu, J. Wang *et al.*, "Isolation and characterization of living circulating tumor cells in patients by immunomagnetic negative enrichment coupled with flow cytometry", Cancer **121**, 17, 3036–3045 (2015).

[83] Luciano, M., M. Erfanzadeh, F. Zhou, H. Zhu, T. Bornhütter, B. Röder, Q. Zhu and C. Brückner, "In vivo photoacoustic tumor tomography using a quinoline-annulated porphyrin as nir molecular contrast agent", Organic & biomolecular chemistry **15**, 4, 972–983 (2017).

[84] Lusk, J. F., C. Miranda, M. Howell, M. Chrest, J. Eshima and B. S. Smith, "Photoacoustic flow system for the detection of ovarian circulating tumor cells utilizing copper sulfide nanoparticles", ACS Biomaterials Science & Engineering **5**, 3, 1553–1560 (2019).

[85] Lusk, J. F., C. Miranda and B. S. Smith, "Ovarian cancer detection using photoacoustic flow cytometry", JoVE (Journal of Visualized Experiments) , 155, e60279 (2020).

[86] Marchetti, C., I. Palaia, M. Giorgini, C. De Medici, R. Iadarola, L. Vertechy, L. Domenici, V. Di Donato, F. Tomao, L. Muzii *et al.*, "Targeted drug delivery via folate receptors in recurrent ovarian cancer: a review", OncoTargets and therapy **7**, 1223 (2014).

[87] Marcus, C. S., G. L. Maxwell, K. M. Darcy, C. A. Hamilton and W. P. McGuire, "Current approaches and challenges in managing and monitoring treatment response in ovarian cancer", Journal of Cancer **5**, 1, 25 (2014).

[88] Matchynski, J. I., R. Manwar, K. J. Kratkiewicz, R. Madangopal, V. A. Lennon, K. M. Makki, A. L. Reppen, A. R. Woznicki, B. T. Hope, S. A. Perrine *et al.*, "Direct measurement of neuronal ensemble activity using photoacoustic imaging in the stimulated fos-lacz transgenic rat brain: a proof-of-principle study", Photoacoustics **24**, 100297 (2021).

[89] Mehrmohammadi, M., S. Joon Yoon, D. Yeager and S. Y Emelianov, "Photoacoustic imaging for cancer detection and staging", Current Molecular Imaging (Discontinued) **2**, 1, 89–105 (2013).

[90] Miranda, C., J. Barkley and B. S. Smith, "Intrauterine photoacoustic and ultrasound imaging probe", Journal of biomedical optics **23**, 4, 046008 (2018).

[91] Miranda, C., S. Sampath Kumar, J. Muthuswamy and B. S. Smith, "Photoacoustic micropipette", Applied Physics Letters **113**, 26, 264103 (2018).

[92] Moon, H., D. Kumar, H. Kim, C. Sim, J.-H. Chang, J.-M. Kim, H. Kim and D.-K. Lim, "Amplified photoacoustic performance and enhanced photothermal stability of reduced graphene oxide coated gold nanorods for sensitive photoacoustic imaging", ACS nano **9**, 3, 2711–2719 (2015).

[93] Moothanchery, M., R. Z. Seeni, C. Xu and M. Pramanik, "In vivo studies of transdermal nanoparticle delivery with microneedles using photoacoustic microscopy", Biomedical Optics Express **8**, 12, 5483–5492 (2017).

[94] Na, S., J. J. Russin, L. Lin, X. Yuan, P. Hu, K. B. Jann, L. Yan, K. Maslov, J. Shi, D. J. Wang *et al.*, "Massively parallel functional photoacoustic computed tomography of the human brain", Nature Biomedical Engineering pp. 1–9 (2021).

[95] Nedosekin, D. A., J. Nolan, C. Cai, S. E. Bourdo, Z. Nima, A. S. Biris and V. P. Zharov, "In vivo noninvasive analysis of graphene nanomaterial pharmacokinetics using photoacoustic flow cytometry", Journal of Applied Toxicology **37**, 11, 1297–1304 (2017).

[96] Nedosekin, D. A., M. Sarimollaoglu, J.-H. Ye, E. I. Galanzha and V. P. Zharov, "In vivo ultra-fast photoacoustic flow cytometry of circulating human melanoma cells using near-infrared high-pulse rate lasers", Cytometry Part A **79**, 10, 825–833 (2011).

[97] Ohnaga, T., Y. Shimada, K. Takata, T. Obata, T. Okumura, T. Nagata, H. Kishi, A. Muraguchi and K. Tsukada, "Capture of esophageal and breast

cancer cells with polymeric microfluidic devices for ctc isolation", Molecular and clinical oncology **4**, 4, 599–602 (2016).

[98] Otani, K. and K. Yamahara, "Development of antibody-carrying microbubbles based on clinically available ultrasound contrast agent for targeted molecular imaging: a preliminary chemical study", Molecular Imaging and Biology **13**, 2, 250–256 (2011).

[99] O'Brien, C. M., K. D. Rood, K. Bhattacharyya, T. Q. DeSouza, S. Sengupta, S. K. Gupta, J. D. Mosley, B. S. Goldschmidt, N. Sharma and J. A. Viator, "Capture of circulating tumor cells using photoacoustic flowmetry and two phase flow", Journal of biomedical optics **17**, 6, 061221 (2012).

[100] Pantel, K. and C. Alix-Panabières, "Circulating tumour cells in cancer patients: challenges and perspectives", Trends in molecular medicine **16**, 9, 398–406 (2010).

[101] Parker, N., M. J. Turk, E. Westrick, J. D. Lewis, P. S. Low and C. P. Leamon, "Folate receptor expression in carcinomas and normal tissues determined by a quantitative radioligand binding assay", Analytical biochemistry **338**, 2, 284–293 (2005).

[102] Poveda, A., S. B. Kaye, R. McCormack, S. Wang, T. Parekh, D. Ricci, C. A. Lebedinsky, J. C. Tercero, P. Zintl and B. J. Monk, "Circulating tumor cells predict progression free survival and overall survival in patients with relapsed/recurrent advanced ovarian cancer", Gynecologic oncology **122**, 3, 567–572 (2011).

[103] Pradeep, S., S. W. Kim, S. Y. Wu, M. Nishimura, P. Chaluvally-Raghavan, T. Miyake, C. V. Pecot, S.-J. Kim, H. J. Choi, F. Z. Bischoff *et al.*, "Hematogenous metastasis of ovarian cancer: rethinking mode of spread", Cancer cell **26**, 1, 77–91 (2014).

[104] Qian, Y., K. D. Piatkevich, B. Mc Larney, A. S. Abdelfattah, S. Mehta, M. H. Murdock, S. Gottschalk, R. S. Molina, W. Zhang, Y. Chen *et al.*, "A genetically encoded near-infrared fluorescent calcium ion indicator", Nature methods **16**, 2, 171–174 (2019).

[105] Qin, C., K. Cheng, K. Chen, X. Hu, Y. Liu, X. Lan, Y. Zhang, H. Liu, Y. Xu, L. Bu *et al.*, "Tyrosinase as a multifunctional reporter gene for photoacoustic/mri/pet triple modality molecular imaging", Scientific reports **3**, 1, 1–8 (2013).

[106] Remington, S. J., "Green fluorescent protein: a perspective", Protein Science **20**, 9, 1509–1519 (2011).

[107] Richie, C. T., L. R. Whitaker, K. W. Whitaker, J. Necarsulmer, H. A. Baldwin, Y. Zhang, L. Fortuno, J. J. Hinkle, P. Koivula, M. J. Henderson *et al.*, "Near-infrared fluorescent protein irfp713 as a reporter protein for optogenetic vectors, a transgenic cre-reporter rat, and other neuronal studies", Journal of neuroscience methods **284**, 1–14 (2017).

[108] Sangha, G. S., E. H. Phillips and C. J. Goergen, "In vivo photoacoustic lipid imaging in mice using the second near-infrared window", Biomedical optics express **8**, 2, 736–742 (2017).

[109] Sano, K., M. Ohashi, K. Kanazaki, N. Ding, J. Deguchi, Y. Kanada, M. Ono and H. Saji, "In vivo photoacoustic imaging of cancer using indocyanine green-labeled monoclonal antibody targeting the epidermal growth factor receptor", Biochemical and biophysical research communications **464**, 3, 820–825 (2015).

[110] Sauer, B., "Functional expression of the cre-lox site-specific recombination system in the yeast saccharomyces cerevisiae", Molecular and cellular biology **7**, 6, 2087–2096 (1987).

[111] Sauer, B. and N. Henderson, "Site-specific dna recombination in mammalian cells by the cre recombinase of bacteriophage p1", Proceedings of the National Academy of Sciences **85**, 14, 5166–5170 (1988).

[112] Sawyer, D. P., A. Bar-Zion, A. Farhadi, S. Shivaei, B. Ling, A. Lee-Gosselin and M. G. Shapiro, "Ultrasensitive ultrasound imaging of gene expression with signal unmixing", Nature Methods **18**, 8, 945–952 (2021).

[113] Shaner, N. C., R. E. Campbell, P. A. Steinbach, B. N. Giepmans, A. E. Palmer and R. Y. Tsien, "Improved monomeric red, orange and yellow fluorescent proteins derived from discosoma sp. red fluorescent protein", Nature biotechnology **22**, 12, 1567–1572 (2004).

[114] Shcherbakova, D. M., "Near-infrared and far-red genetically encoded indicators of neuronal activity", Journal of Neuroscience Methods **362**, 109314 (2021).

[115] Shi, S., X. Wen, T. Li, X. Wen, Q. Cao, X. Liu, Y. Liu, M. D. Pagel and C. Li, "Thermosensitive biodegradable copper sulfide nanoparticles for real-time multispectral optoacoustic tomography", ACS applied bio materials **2**, 8, 3203–3211 (2019).

[116] Shimomura, O., "Structure of the chromophore of aequorea green fluorescent protein", FEBS letters **104**, 2, 220–222 (1979).

[117] Shu, X., H. Li, B. Dong, C. Sun and H. F. Zhang, "Quantifying melanin concentration in retinal pigment epithelium using broadband photoacoustic microscopy", Biomedical optics express **8**, 6, 2851–2865 (2017).

[118] Siegel, R. L., K. D. Miller, H. E. Fuchs and A. Jemal, "Cancer statistics, 2021", CA: A Cancer Journal for Clinicians **71**, 1, 7–33 (2021).

[119] Singh, P., S. Pandit, V. Mokkapati, A. Garg, V. Ravikumar and I. Mijakovic, "Gold nanoparticles in diagnostics and therapeutics for human cancer", International journal of molecular sciences **19**, 7, 1979 (2018).

[120] Siwowska, K., R. M. Schmid, S. Cohrs, R. Schibli and C. Müller, "Folate receptor-positive gynecological cancer cells: In vitro and in vivo characterization", Pharmaceuticals **10**, 3, 72 (2017).

[121] Stein, E. W., K. Maslov and L. V. Wang, "Noninvasive, in vivo imaging of the mouse brain using photoacoustic microscopy", Journal of applied physics **105**, 10, 102027 (2009).

[122] Stewart, C., C. Ralyea and S. Lockwood, "Ovarian cancer: an integrated review", in "Seminars in oncology nursing", vol. 35, pp. 151–156 (Elsevier, 2019).

[123] Szymczak, L. C., H.-Y. Kuo and M. Mrksich, "Peptide arrays: development and application", Analytical chemistry **90**, 1, 266 (2018).

[124] Takao, M. and K. Takeda, "Enumeration, characterization, and collection of intact circulating tumor cells by cross contamination-free flow cytometry", Cytometry Part A **79**, 2, 107–117 (2011).

[125] Tsien, R. Y., "The green fluorescent protein", Annual review of biochemistry **67**, 1, 509–544 (1998).

[126] Tuerk, C. and L. Gold, "Systematic evolution of ligands by exponential enrichment: Rna ligands to bacteriophage t4 dna polymerase", science **249**, 4968, 505–510 (1990).

[127] Turtaev, S., I. T. Leite, T. Altwegg-Boussac, J. M. Pakan, N. L. Rochefort and T. Čižmár, "High-fidelity multimode fibre-based endoscopy for deep brain in vivo imaging", Light: Science & Applications **7**, 1, 1–8 (2018).

[128] Ugolini, G., "Rabies virus as a transneuronal tracer of neuronal connections", Advances in virus research **79**, 165–202 (2011).

[129] Viator, J. A., S. Gupta, B. S. Goldschmidt, K. Bhattacharyya, R. Kannan, R. Shukla, P. S. Dale, E. Boote and K. Katti, "Gold nanoparticle mediated detection of prostate cancer cells using photoacoustic flowmetry with optical reflectance", Journal of biomedical nanotechnology **6**, 2, 187–191 (2010).

[130] Viator, J. A., M. Hazur, A. Sajewski, A. Tarhini, M. E. Sanders and R. H. Edgar, "Photoacoustic detection of circulating melanoma cells in late stage patients", Journal of innovative optical health sciences **13**, 06, 2050023 (2020).

[131] Wang, H., C. Liu, X. Gong, D. Hu, R. Lin, Z. Sheng, C. Zheng, M. Yan, J. Chen, L. Cai *et al.*, "In vivo photoacoustic molecular imaging of breast carcinoma with folate receptor-targeted indocyanine green nanoprobes", Nanoscale **6**, 23, 14270–14279 (2014).

[132] Wang, L. V. and S. Hu, "Photoacoustic tomography: in vivo imaging from organelles to organs", science **335**, 6075, 1458–1462 (2012).

[133] Wang, L. V. and J. Yao, "A practical guide to photoacoustic tomography in the life sciences", Nature methods **13**, 8, 627–638 (2016).

[134] Watanabe, M., Y. Uehara, N. Yamashita, Y. Fujimura, K. Nishio, T. Sawada, K. Takeda, F. Koizumi and Y. Koh, "Multicolor detection of rare tumor cells in blood using a novel flow cytometry-based system", Cytometry Part A **85**, 3, 206–213 (2014).

[135] Weber, J., P. C. Beard and S. E. Bohndiek, "Contrast agents for molecular photoacoustic imaging", Nature methods **13**, 8, 639–650 (2016).

[136] Wilson, K. E., S. V. Bachawal, L. Abou-Elkacem, K. Jensen, S. Machtaler, L. Tian and J. K. Willmann, "Spectroscopic photoacoustic molecular imaging of breast cancer using a b7-h3-targeted icg contrast agent", Theranostics **7**, 6, 1463 (2017).

[137] Wong, T. T., R. Zhang, P. Hai, C. Zhang, M. A. Pleitez, R. L. Aft, D. V. Novack and L. V. Wang, "Fast label-free multilayered histology-like imaging of human breast cancer by photoacoustic microscopy", Science advances **3**, 5, e1602168 (2017).

[138] Wray, P., L. Lin, P. Hu and L. V. Wang, "Photoacoustic computed tomography of human extremities", Journal of biomedical optics **24**, 2, 026003 (2019).

[139] Wu, C.-H., I.-J. Liu, R.-M. Lu and H.-C. Wu, "Advancement and applications of peptide phage display technology in biomedical science", Journal of biomedical science **23**, 1, 1–14 (2016).

[140] Wu, D., L. Huang, M. S. Jiang and H. Jiang, "Contrast agents for photoacoustic and thermoacoustic imaging: a review", International journal of molecular sciences **15**, 12, 23616–23639 (2014).

[141] Xia, J., J. Yao and L. V. Wang, "Photoacoustic tomography: principles and advances", Electromagnetic waves (Cambridge, Mass.) **147**, 1 (2014).

[142] Xu, M. and L. V. Wang, "Photoacoustic imaging in biomedicine", Review of scientific instruments **77**, 4, 041101 (2006).

[143] Xu, Z., Y. Pan, N. Chen, S. Zeng, L. Liu, R. Gao, J. Zhang, C. Fang, L. Song and C. Liu, "Visualizing tumor angiogenesis and boundary with polygon-scanning multiscale photoacoustic microscopy", Photoacoustics p. 100342 (2022).

[144] Yang, C., R. Tian, T. Liu and G. Liu, "Mri reporter genes for noninvasive molecular imaging", Molecules **21**, 5, 580 (2016).

[145] Yang, J. M., C. Favazza, J. Yao, R. Chen, Q. Zhou, K. K. Shung and L. V. Wang, "Three-dimensional photoacoustic endoscopic imaging of the rabbit esophagus", PLoS One **10**, 4, e0120269 (2015).

[146] Yang, J.-M., K. Maslov, H.-C. Yang, Q. Zhou, K. K. Shung and L. V. Wang, "Photoacoustic endoscopy", Optics letters **34**, 10, 1591–1593 (2009).

[147] Yang, W. and R. Yuste, "In vivo imaging of neural activity", Nature methods **14**, 4, 349–359 (2017).

[148] Yao, D.-K., K. Maslov, K. K. Shung, Q. Zhou and L. V. Wang, "In vivo label-free photoacoustic microscopy of cell nuclei by excitation of dna and rna", Optics letters **35**, 24, 4139–4141 (2010).

[149] Yao, J., A. A. Kaberniuk, L. Li, D. M. Shcherbakova, R. Zhang, L. Wang, G. Li, V. V. Verkhusha and L. V. Wang, "Multiscale photoacoustic tomography using reversibly switchable bacterial phytochrome as a near-infrared photochromic probe", Nature methods **13**, 1, 67–73 (2016).

[150] Yao, J., L. Wang, J.-M. Yang, K. I. Maslov, T. T. Wong, L. Li, C.-H. Huang, J. Zou and L. V. Wang, "High-speed label-free functional photoacoustic microscopy of mouse brain in action", Nature methods **12**, 5, 407–410 (2015).

[151] Yao, J. and L. V. Wang, "Photoacoustic tomography: fundamentals, advances and prospects", Contrast media & molecular imaging **6**, 5, 332–345 (2011).

[152] Yao, J. and L. V. Wang, "Photoacoustic microscopy", Laser & photonics reviews **7**, 5, 758–778 (2013).

[153] Yin, C., G. Wen, C. Liu, B. Yang, S. Lin, J. Huang, P. Zhao, S. H. D. Wong, K. Zhang, X. Chen *et al.*, "Organic semiconducting polymer nanoparticles for photoacoustic labeling and tracking of stem cells in the second near-infrared window", ACS nano **12**, 12, 12201–12211 (2018).

[154] Yoon, T.-J. and Y.-S. Cho, "Recent advances in photoacoustic endoscopy", World journal of gastrointestinal endoscopy **5**, 11, 534 (2013).

[155] Zerda, A. d. l., Z. Liu, S. Bodapati, R. Teed, S. Vaithilingam, B. T. Khuri-Yakub, X. Chen, H. Dai and S. S. Gambhir, "Ultrahigh sensitivity carbon nanotube agents for photoacoustic molecular imaging in living mice", Nano letters **10**, 6, 2168–2172 (2010).

[156] Zhang, C., R. Kimura, L. Abou-Elkacem, J. Levi, L. Xu and S. S. Gambhir, "A cystine knot peptide targeting integrin $\alpha v\beta 6$ for photoacoustic and fluorescence imaging of tumors in living subjects", Journal of Nuclear Medicine **57**, 10, 1629–1634 (2016).

[157] Zhang, C., K. Maslov and L. V. Wang, "Subwavelength-resolution label-free photoacoustic microscopy of optical absorption in vivo", Optics letters **35**, 19, 3195–3197 (2010).

[158] Zhang, C., Y. S. Zhang, D.-K. Yao, Y. Xia and L. V. Wang, "Label-free photoacoustic microscopy of cytochromes", Journal of biomedical optics **18**, 2, 020504 (2013).

[159] Zhang, H., J. Li, Y. Hu, M. Shen, X. Shi and G. Zhang, "Folic acid-targeted iron oxide nanoparticles as contrast agents for magnetic resonance imaging of human ovarian cancer", Journal of ovarian research **9**, 1, 1–8 (2016).

[160] Zhang, H. F., K. Maslov, G. Stoica and L. V. Wang, "Functional photoacoustic microscopy for high-resolution and noninvasive in vivo imaging", Nature biotechnology **24**, 7, 848–851 (2006).

[161] Zhang, J., L. P. Smaga, N. S. R. Satyavolu, J. Chan and Y. Lu, "Dna aptamer-based activatable probes for photoacoustic imaging in living mice", Journal of the American Chemical Society **139**, 48, 17225–17228 (2017).

[162] Zhang, P., L. Li, L. Lin, P. Hu, J. Shi, Y. He, L. Zhu, Y. Zhou and L. V. Wang, "High-resolution deep functional imaging of the whole mouse brain by photoacoustic computed tomography in vivo", Journal of biophotonics **11**, 1, e201700024 (2018).

[163] Zhang, X., S. Bloch, W. Akers and S. Achilefu, "Near-infrared molecular probes for in vivo imaging", Current protocols in cytometry **60**, 1, 12–27 (2012).

[164] Zharov, V. P., E. I. Galanzha, E. V. Shashkov, J.-W. Kim, N. G. Khlebtsov and V. V. Tuchin, "Photoacoustic flow cytometry: principle and application for real-time detection of circulating single nanoparticles, pathogens, and contrast dyes in vivo", Journal of biomedical optics **12**, 5, 051503 (2007).

[165] Zhou, M., S. Song, J. Zhao, M. Tian and C. Li, "Theranostic cus nanoparticles targeting folate receptors for pet image-guided photothermal therapy", Journal of Materials Chemistry B **3**, 46, 8939–8948 (2015).

[166] Zhou, Y., B. Bian, X. Yuan, G. Xie, Y. Ma and L. Shen, "Prognostic value of circulating tumor cells in ovarian cancer: a meta-analysis", PLoS One **10**, 6, e0130873 (2015).